The profile of a highly selective quaternized pyrrolidine betaine $\alpha_v\beta_6$ integrin inhibitor - (3*S*)-3-(3-(3,5-dimethyl-1*H*-pyrazol-1-yl)phenyl)-4-((1*S* and 1*R*,3*R*)-1-methyl-3-(2-(5,6,7,8-tetrahydro-1,8-naphthyridin-2-yl)ethyl)pyrrolidin-1-ium-1-yl)butanoate synthesized by a stereoselective methylation

Tim N. Barrett,[a] Jonathan A. Taylor,[a]* Daniel Barker,[a] Panayiotis A. Procopiou,[a] James D.F. Thompson,[a, b] John Barrett,[a] Joelle Le,[a] Sean M. Lynn,[a] Peter Pogany,[a] Cassie Pratley,[a] John M. Pritchard, [a] James A. Roper, [a] James E. Rowedder,[a] Robert J. Slack, [a] Giovanni Vitulli,[a] Simon J. F. Macdonald,[a] and William J. Kerr[b]

[a]*Medicinal Science & Technology, GlaxoSmithKline Medicines Research Centre, Gunnels Wood Road, Stevenage, SG1 2NY, United Kingdom*

[b]*Department of Pure & Applied Chemistry, University of Strathclyde, 295 Cathedral St, Glasgow, G1 1XL, UK*

* To whom correspondence should be addressed. E-mail: jonathan.a.taylor@gsk.com

Keywords: $\alpha_v\beta_6$ integrin, inhibitor, betaine, conformation, idiopathic pulmonary fibrosis

Abstract: A quaternary ammonium betaine **7** is described which shows exceptional potency and selectivity (1.4 - >3 logs) for the $\alpha_v\beta_6$ integrin receptor over the other α_v integrins as determined in cell adhesion assays. **7** is prepared by a remarkably stereoselective methylation the origins of which are discussed. The chemical, biological, physicochemical and pharmacokinetic properties of **7** and its docking into $\alpha_v\beta_6$ are described along with related analogs.

Introduction

Idiopathic pulmonary fibrosis (IPF) is a chronic lung disease the etiology of which is unknown but is thought to result from epithelial cell damage. Dysregulated repair processes to resolve the damage results in excessive collagen deposition in the lungs which leads to a progressive loss of lung function. [1] The average life-expectancy of IPF patients from the time of diagnosis is less than 3 years.[2,3] Treatment of the disease was limited until pirfenidone **1** and nintedanib **2** were approved in 2014 (Fig. 1).[4] Both compounds are administered orally at high doses and due to various side effects can exhibit low patient compliance and so improved and effective new therapies for the treatment of IPF are therefore needed and is an area of active research.[5]

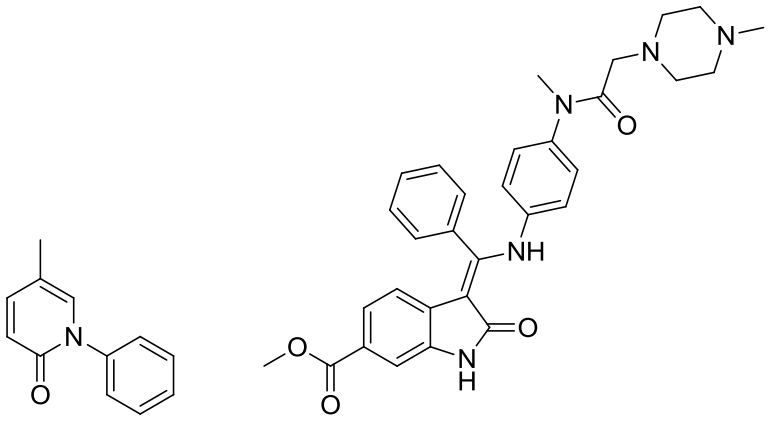

Pirfenidone 1
(Roche)

Nintedanib 2
(Boehringer-Ingelheim)

Figure 1. The structures of the two currently approved drugs for the treatment of IPF Pirfenidone and Nintedanib.

Our own work in this area has focused on inhibitors of the integrin $\alpha_v\beta_6$ receptor. Integrins are a family of transmembrane, heterodimeric cell adhesion receptors that connect cell-surface ligands to the extracellular matrix and play a pivotal role in communication.[6] The integrin superfamily is divided into several subfamilies, including collagen, laminin, leukocyte-specific

and arginyl-glycinyl-aspartic acid (RGD) receptors. Inhibitors of the $\alpha_{IIb}\beta_3$ receptor - an RGD integrin receptor – are marketed drugs for various cardiovascular indications. The α_v subset of the RGD integrins ($\alpha_v\beta_1$, $\alpha_v\beta_3$, $\alpha_v\beta_5$, $\alpha_v\beta_6$ and $\alpha_v\beta_8$) have been explored for the treatment of a number of diseases such as cancer, inflammatory diseases, multiple sclerosis, osteoporosis and organ fibrosis[7] and several reviews on integrin-based therapeutic agents have recently been published.[8] [9,10]

There is now considerable literature for antibody and small molecule (such as **3**, **4** and **5** (Fig. 2)) [10,11,12,13] pan α_v inhibitors (defined as those inhibiting most or all the av sub-family of receptors) which describes target validation studies for fibrotic diseases (see reference 10 for leading references) and cancer with **3** having been clinically evaluated.[14]

In addition, there is now excellent target validation evidence for selective inhibition of the integrin $\alpha_v\beta_6$ itself for fibrotic diseases[10,15] with both a specific $\alpha_v\beta_6$ humanized monoclonal antibody BG00011, also known as STX-100,[10,16,] and the GSK small molecule **6** (also known as GSK3008348) undergoing clinical trials for the treatment of IPF.[17]

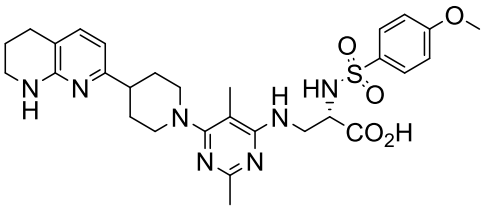

3 presumed structure of GLPG0187

Integrin	IC_{50}
αvβ1	1.3nM
αvβ3	3.7nM
αvβ5	2.0nM
αvβ6	1.4nM
αvβ8	1.2nM

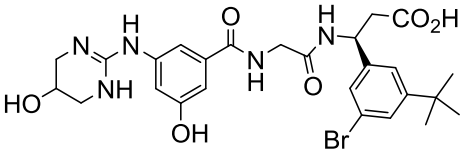

4 CWHM 12

Integrin	IC_{50}
αvβ1	1.8nM
αvβ3	0.8nM
αvβ5	61nM
αvβ6	1.5nM
αvβ8	0.2nM

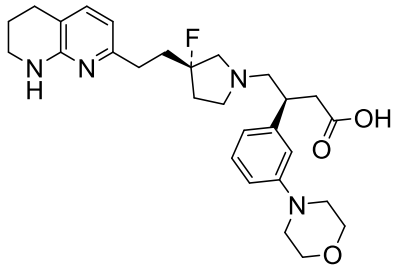

5 Example 1

Integrin	pIC_{50}
αvβ1	7.0
αvβ3	6.9
αvβ5	7.1
αvβ6	**8.0**
αvβ8	7.6

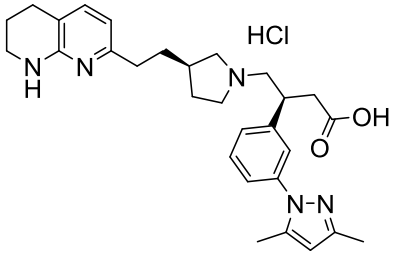

6 GSK3008348

Integrin	pIC_{50}
αvβ1	7.3
αvβ3	6.0
αvβ5	6.9
αvβ6	**8.4**
αvβ8	7.7

Figure 2. Structures of pan integrin inhibitors **3**-**5** and a selective $\alpha_v\beta_6$ inhibitor **6**. Both **3** and **6** are or have been clinically evaluated for cancer and IPF respectively. All the quoted data are from reference 10.

Compound **6** is a selective, high-affinity small-molecule $\alpha_v\beta_6$ integrin inhibitor with excellent aqueous solubility which is suitable for dosing by inhalation.[15] As part of our structure activity relationship (SAR) studies around **6** and also as part determining the absolute configuration of **6**,[18] quaternary ammonium salts of the central pyrrolidine were prepared. These are remarkable compounds. They can be made stereoselectively and show outstanding selectivity for $\alpha_v\beta_6$ over the other α_v integrins namely $\alpha_v\beta_1$, $\alpha_v\beta_3$, $\alpha_v\beta_5$ and $\alpha_v\beta_8$. To the best of our knowledge at the time of writing, the methyl compound **7** is the most selective small molecule (including

peptides[12]) known in the literature and may be of value for target validation studies. We report here the synthesis, characterization, properties and biological activities of quaternary ammonium salts of **6** and related analogs. Preliminary pharmacokinetic studies are also described. The overall profile of **7** that is described is consistent with an inhaled therapeutic for IPF.

Results and Discussion

Synthetic considerations

Alkylating 6 The measured pK_a's for the carboxylic acid group of **6** is 4.07, for the tetrahydronaphthyridine 7.38 and for the pyrrolidine 9.50.[15] It is therefore expected that **6** will exist in the zwitterionic form. These studies commenced with the free base of **6,**[18] being warmed with excess methyl iodide (20 equiv.) at 50°C for 5 min in dichloromethane in a sealed vessel (Scheme 1, Figure 3). In the absence of any additional base, the hydrogen iodide generated in the reaction was expected to form either betaine-tetrahydronaphthyridine hydroioidide[19] **X** or the zwitterionic quaternary ammonium salt **Y**. The crude material was purified by reverse-phase HPLC under basic conditions (10 mM aqueous ammonium bicarbonate containing 0.1% aqueous ammonia) forming the ammonium salt of the carboxylic acid **Z**. Upon evaporation of the solvent from the fractions containing product, any ammonia and ammonium bicarbonate present in the eluant and also the ammonium counterion of the carboxylic acid are removed allowing the isolation of the product as a mixture of diastereomeric betaines **7** and **8** in about a 9:1 (89:11) ratio in 77% yield. The diastereomeric ratio was determined by HPLC on a Chiralcel OD-H column, and by ^{1}H NMR spectroscopy (see later).

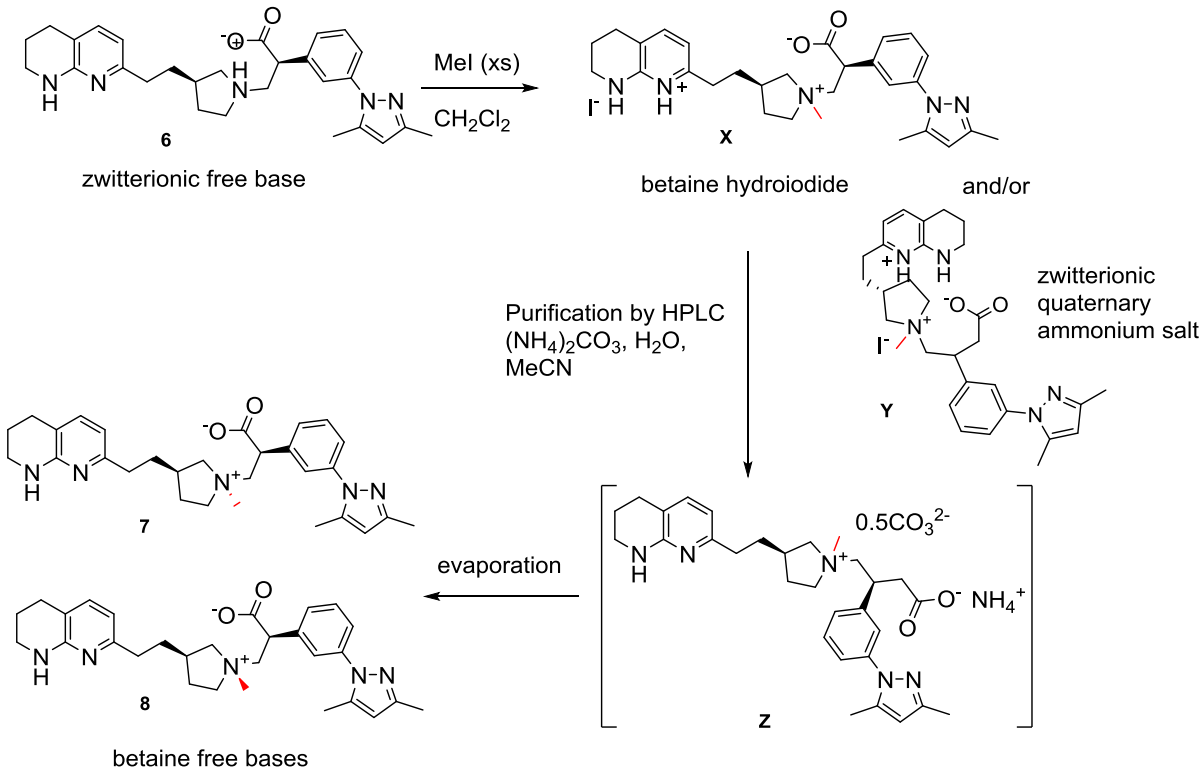

Scheme 1 General reaction scheme for quaternization of the pyrrolidine nitrogen and purification

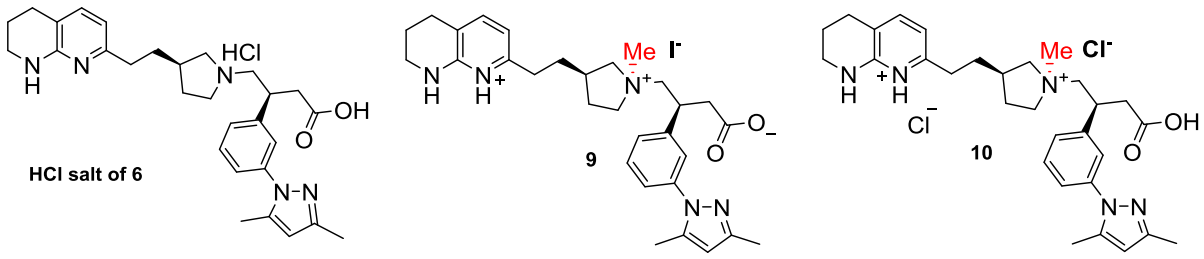

Figure 3. The general reaction scheme and structures of various compounds and their salt forms

Having observed the stereoselective alkylation of zwitterionic **6** at 50°C, we attempted to improve the diastereoselectivity by examining the alkylation at 20°C. As it was more readily available, **6** hydrochloride (containing 1.6 equivalents of hydrogen chloride) was used in the presence of a 1.6 molar equivalent amount of solid potassium carbonate to generate the

zwitterion *in situ*, and stirred with excess methyl iodide (10 equiv.), at 20°C for 69 h. After purification by reverse-phase HPLC as described above, the major diastereomer was obtained in 83% yield. This product was a single diastereomer established both by HPLC on a chiral support, and by ^{1}H- and ^{13}C-NMR spectroscopy. The stereochemistry of the methyl group of the pyrrolidinium group was established by 2D ROESY, where a correlation was observed between the *N*-Me singlet at 2.83 ppm and the pyrrolidine 3-H in the multiplet at 2.51-2.39 ppm, and by 1D ROESY where irradiation at 2.41 ppm provided nOe enhancement of the *N*-Me peak at 2.83 ppm (Fig. 4), confirming that both are on the same face of the pyrrolidine ring. This therefore confirmed the configuration of the quaternary nitrogen stereocenter as (*S*).

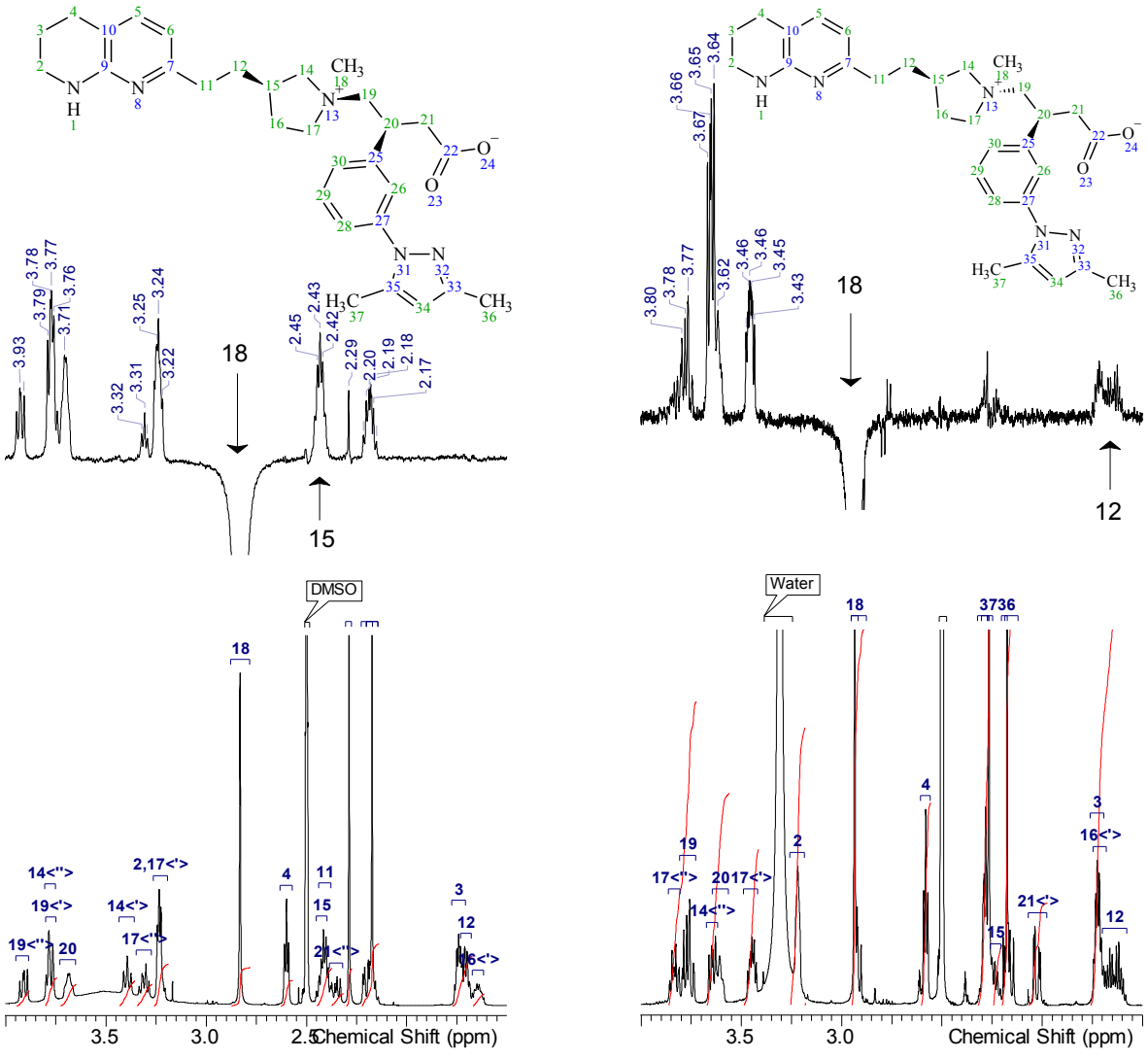

Figure 4. Left hand panels: Part of the ^{1}H NMR spectrum of **7** in DMSO-d_6 (lower left panel) and an nOe (upper left panel) resulting from irradiation of the quaternary methyl group (labelled 18) showing enhancement of H-15 (arrowed) thus confirming the relative stereochemistry of the quaternary nitrogen of **7**. Right hand panels: Part of the ^{1}H NMR spectrum of **8** in DMSO-d_6 (lower right panel) and an nOe (upper right panel) resulting from irradiation of the quaternary methyl group (labelled 18) showing enhancement of H- 12 (arrowed) and no enhancement of H-15 thus confirming the relative stereochemistry of the quaternary nitrogen of **8**. Images of the full spectra are provided in the Supporting Information.

The alkylation of **6** with excess methyl iodide was also examined in other solvents (data not shown), such as DMF and alcohols and although the reactions proceeded to completion, mixtures of polyalkylated products were obtained. As a consequence, all other alkylation experiments were conducted in dichloromethane.

The methylation proved difficult to scale-up leading to lower yields and incomplete reactions so larger quantities of **7** were obtained by pooling the crude product from several reactions and purifying by supercritical fluid chromatography (SFC) using aqueous ammonia in methanol as eluant to provide the betaine **7** in 65% yield. It is possible to generate the pyrrolidinium iodide salt **9** under the same reaction conditions when purification is carried out under normal phase chromatography conditions by using silica and eluting with methanol in dichloromethane. Other salts of **7** can be obtained by adding a stoichiometric amount of acid such as hydrogen chloride to **7** to give **10**.

Despite various attempts, we were unable to obtain a pure sample of the minor diastereomer of the methylated product **8** from the procedure described above. Instead we envisaged methylation of the methyl ester **11** hypothesizing that the ester **11** might have a more open and

extended confirmation compared to the acid **6** allowing methyl iodide to approach from both faces and thus provide a mixture of isomers with an improved ratio for the minor isomer. In fact, treatment of **11** with 1.5 equiv. of methyl iodide in dichloromethane and in the presence of potassium carbonate as base provided about a 2.5:1 (by NMR) mixture of diastereomers of **12** and **13** in 64% isolated yield (Scheme 2). The esters were hydrolysed using lithium hydroxide and after acidification, purified by mass-directed auto-preparative HPLC (MDAP) under basic conditions (aqueous ammonia in 10 mM ammonium bicarbonate buffer) to give a mixture of diastereomers (2.6:1 by NMR). With more of each isomer present in the mixture, separation of the diastereomers proved possible by HPLC on a chiral support to give **8** in 8% (anal. chiral HPLC RT=14.2 min, 100%) and **7** in 23% yield (anal. chiral HPLC RT=16.7 min, 98.2%). The stereochemistry of **8** was established as before by nOe. Irradiation of the *N*-Me at 2.93 ppm showed nOe enhancement of the methylene at 1.64 ppm in the ethyl side-chain containing the naphthyridine ring (Fig. 4).

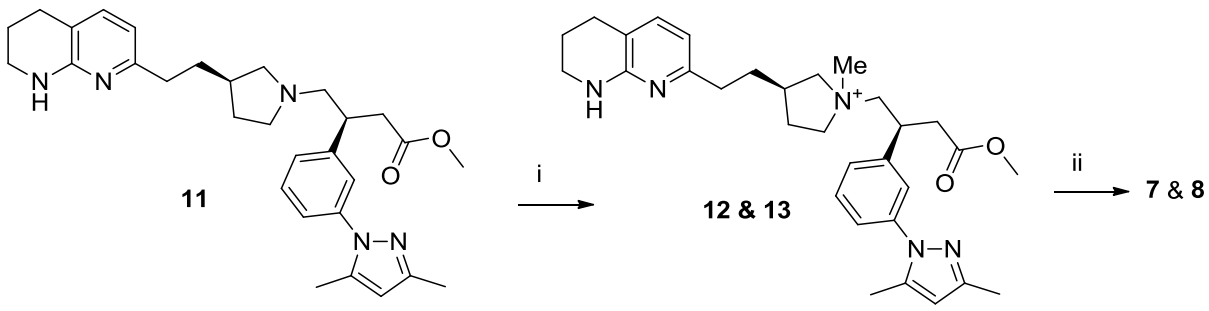

Scheme 2. *Reagents and conditions*: i) MeI (1.5 equiv.), K_2CO_3, DCM, 64%; ii) aq. LiOH (3 equiv.), THF, **7** (23%) and **8** (8%).

The *N*-ethyl analog **14** as the diformate salt was prepared from **6** and ethyl iodide in dichloromethane in about 10% yield (Scheme 3). The configuration was again established by NMR. Finally, three potent $\alpha_v\beta_6$ inhibitors and analogs of **6,**[15] the morpholine **15a**, the 5-

methylpyrazole **15b** and the tetrahydrofuran **15c** were alkylated with methyl iodide as before to provide the corresponding methylpyrrolidine betaines **16a**, **16b** and **16c** in 15, 35 and 11% yield respectively (Scheme 3) with the structures established by NMR studies. The last two compounds were obtained as diastereomeric mixtures in the ratio of 5:1, 3:1 and 4:1 respectively.

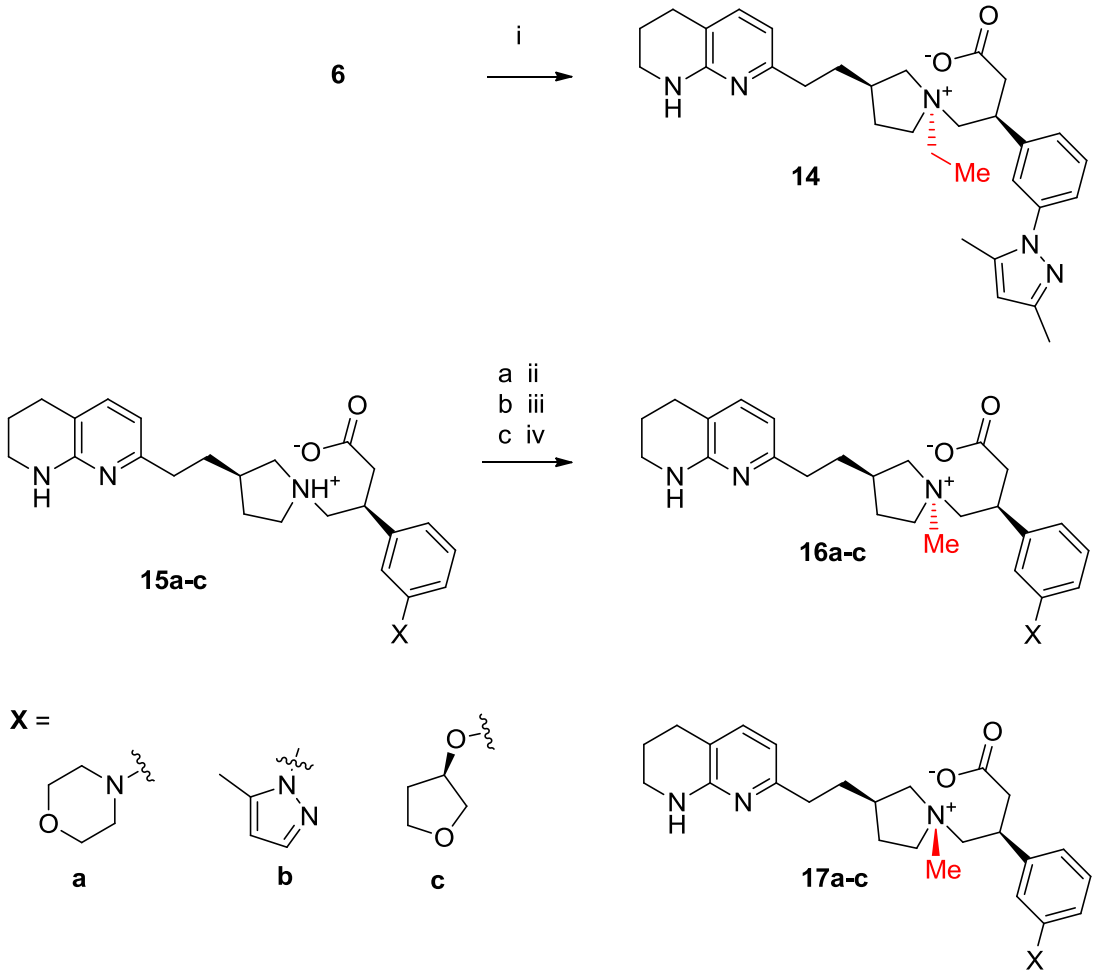

Input	Base	RI	Yield	Ratio of isomers
6 zwitterion free base	-	EtI	10% of diformate salt	**14** only isolated
15a zwitterion free base	-	MeI	15% of the betaines	**16a:17a** 5:1
15b hydrochloride	K_2CO_3	MeI	35% of the betaines	**16b**:**17b** 3:1
15c zwitterion free base	K_2CO_3	MeI	11% of the betaines	**16c**:**17c** 4:1

Scheme 3 *Reagents and conditions*: i) **6 (**zwitterion free base), EtI (7 equiv.), DCM, 10%; ii) **15a (**zwitterion free base), MeI, DCM, 15%; iii) **15b** (hydrochloride) MeI, K_2CO_3, DCM, 35%; iv) **15c** (zwitterion free base), MeI, K_2CO_3, DCM, 11%.

The stereoselectivity of the alkylation When the acids (in whatever salt form) are used as the substrates, there is a clear facial selectivity for alkylation varying from at least 3:1 for **15b** to 9:1 for **6**. We hypothesize that in a non-polar solvent such as dichloromethane the internal zwitterion between the carboxylic acid and pyrrolidine amine (as in **6** zwitterionic free base in Scheme 1) forms a pseudo ring system which confers differential facial selectivity with the alkylating agent approaching predominantly from the less-hindered face.

One supporting strands of evidence for this hypothesis comes from the optical rotations previously reported.[18] There is a significant difference in the optical rotation of **6** as the zwitterionic free base which is $[\alpha]_D^{20} = +46^o$ (c=1.00 in EtOH) compared to **6** as the hydrochloride which is $[\alpha]_D^{20} = -22^o$ (c=1.23 in EtOH).[20] This suggests that the two salt forms have different conformations – the zwitterion being pseudo cyclic and the hydrochloride more extended as shown in Figure 3. These rotation values are both measured in ethanol – a polar protic solvent more likely to stabilize ionized or partially ionized species. In a less polar solvent such as dichloromethane, the pyrrolidinium salt and carboxylate are even more likely to associate in some way (either intermolecularly or more probably intramolecularly) to minimise the polar surface area.

Attempts were also made to rationalize the high diastereoselectivity of the methylation of **6** to give **7** using quantum chemical calculations. The conformer generation of **6** was performed using Macromodel,[21] and geometry optimisation of the resulting conformations was carried out using Gaussian 16,[22] using the B3LYP-D3, 6-31+G** level of theory and a polarisable continuum model (PCM) solvation model with CH_2Cl_2.[23,24,25] The intramolecular hydrogen

bonds and π-π interactions visible in all conformations cause noticeable coiling in the lowest-energy structures in both the gas phase and in implicit CH_2Cl_2 solution (Fig. 5). The minimum solution phase energy conformation of **6** in its anionic form (likely to predominate in the presence of K_2CO_3) is shown in Fig. 5). The tightly coiled conformation leaves only one face of the pyrrolidine moiety exposed to the solvent and electrophile approach. Unfortunately, *N*-methylation of this exposed face would lead to the formation of **8** rather than **7**, so rationalizing the diastereoselectivity of this reaction using the preferred low energy conformation of the starting material was unsuccessful.

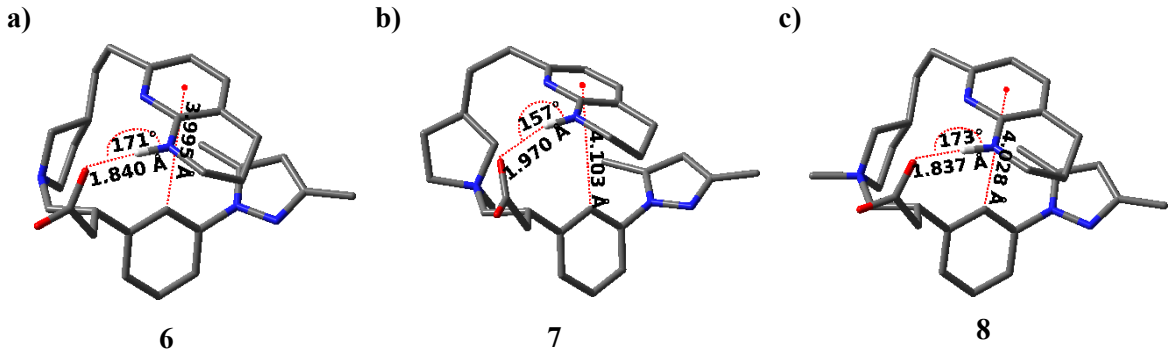

Figure 5 The lowest energy conformations of compounds **6**, **7** and **8,** obtained by conformation search and subsequent geometry optimisation using the B3LYP-D3, 6-31+G** level of theory and a PCM solvation model with CH_2Cl_2. For each compound, an intramolecular hydrogen bonding interaction is exhibited between the carboxylate and the tetrahydronaphthyridine group, as well as π-π interactions, resulting in a coiled conformation. **a)** The minimum energy conformation of the anionic form of **6**, with only one face of the pyrrolidine ring solvent-exposed. Methylation of this face would lead to the formation of **8** rather than **7**, which is not observed experimentally. **b)** The lowest energy conformation of **7**. **c)** The lowest energy conformation of **8**. The calculated solution phase energy of this conformation of **8** is 14.08 kJ mol^{-1} lower than of this conformation of **7**, which would suggest that there is a thermodynamic preference for the formation of **8** over **7** although this is not observed experimentally.

Additionally, the minimum energy conformations of the two possible products **7** and **8** were calculated, to establish whether the selectivity might derive from a thermodynamic preference for the formation of **7** over **8**. Unfortunately, the calculations showed that **8** is energetically more favoured over **7** by 14.08 kJ mol^{-1} **(Figure 5 b) and c))**. The hydrogen bond distances and orientations are also more favorable for **6** and **8** than **7**, and it is noteworthy that the lowest energy conformations of **6** and **8** are similar. This approach therefore also does not successfully explain the stereoselective alkylations that have been observed experimentally. This may be because the model does not consider the explicit interactions between the solvent or counterions and the molecule or molecular self-association.

However, an alternative explanation for the failure of this computational investigation to provide an explanation is that the particular conformation arises from the intermoledcular association of more than one molecule of **6**. NMR studies were therefore conducted, varying the concentration of **6**, as a change in chemical shift might be expected if self-association is occuring in solution.[26]

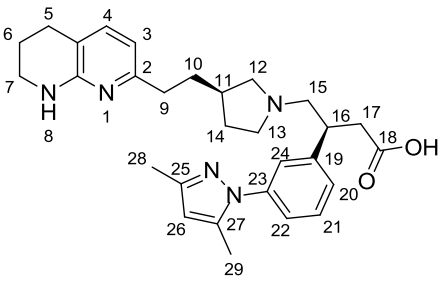

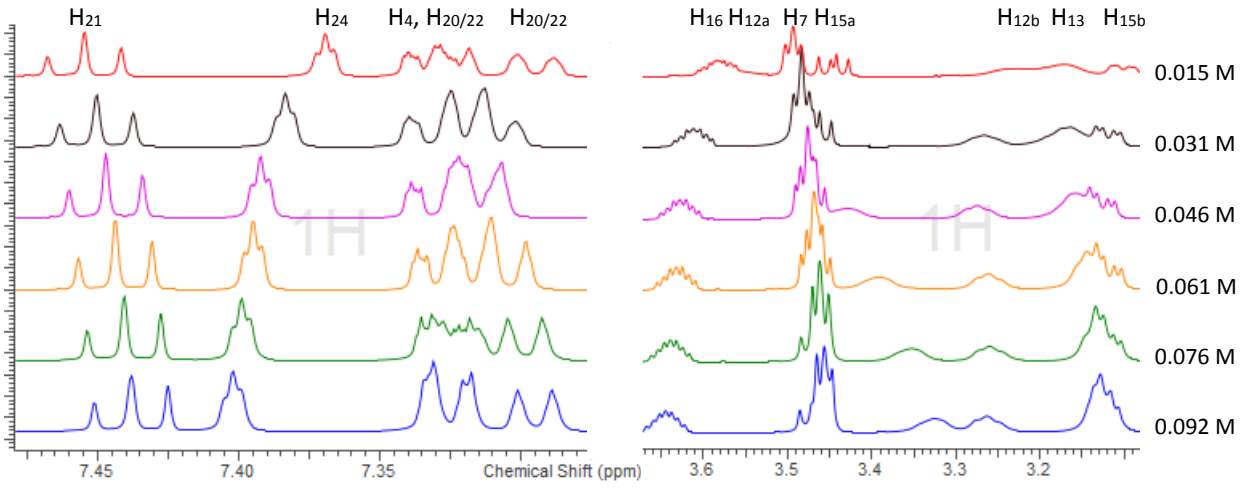

Figure 6 Two excerpts from the ^{1}H- NMR spectra of **6** in CD_2Cl_2 with K_2CO_3 at a range of concentrations (labelled on the right), with a concentration-dependent shift in many of the peaks being observed. (Full annotated spectra are provided in the Supporting Information). The peaks for the spectrum measured at 0.015 M are labelled, with the labels corresponding to protons numbered in the figure of **6** above. Protons from across the whole molecule are affected by the dilution. This suggests some level of intermolecular self-association which is not readily included into the computational calculations described above.

In order to mimic the reaction conditions, the NMR spectra were measured in deuterated dichloromethane in the presence of potassium carbonate in the same stoichiometry as in the methylation reaction. Six different concentrations were measured, from 0.092 M (the reaction concentration) to 0.015 M. Two representative excerpts from the ^{1}H NMR spectra measured are shown (Figure 6), with the spectra at the different concentrations overlaid to aid comparison. There is a marked shift of many of the protons in the spectra as the concentration changes, which implies self-association of the compound. The diastereoselectivity of the methylation of **6** may, therefore, be the result of a conformation which arises from the formation of a dimer, trimer or higher aggregate of **6**. This could explain why the computational work with only one molecule of **6** in consideration is not concordant with the experimentally observed selectivity. Further studies in this area are ongoing and will be reported in due course.

Biological activity

Based on our previous work,[15] a selection of substituted aryl pyrrolidine derivatives were quaternized. The binding affinity and selectivity of the betaines **7**, **8**, **14** and **16a-c** together

with their respective parents **6**, **15a-c** were determined in cell adhesion assays against the α_v integrins ($\alpha_v\beta_1$, $\alpha_v\beta_3$, $\alpha_v\beta_5$, $\alpha_v\beta_6$ and $\alpha_v\beta_8$) (Table 1).[27]

P'lidine subst^n	Aryl subst^n	Cmpd	$\alpha_v\beta_6$ pIC_{50}	$\alpha_v\beta_1$ pIC_{50}	$\alpha_v\beta_3$ pIC_{50}	$\alpha_v\beta_5$ pIC_{50}	$\alpha_v\beta_8$ pIC_{50}	clogP	Chrom $logD_{7.4}$
-	Dimethyl-pyrazolo	**6**	8.4	7.3	6.0	6.9	7.8	2.7	2.8
S-Me	"	**7**	8.5	6.2	5.2	6.3	7.1	-2.0	2.5
R-Me	"	**8**	8.5	5.7	<5.0	6.0	7.2	-2.0	2.4
S-Et	"	**14**	7.4	5.3	nt	<5.0	5.9	-1.5	2.8
-	Morpho-lino	**15a**	8.4	6.6	6.2	7.3	7.8	1.6	2.3
5:1 *S:R*-Me	"	**16a**	7.9	6.1	5.3	6.6	6.9	-3.1	1.8
-	Methyl-pyrazolo	**15b**	8.7	7.3	6.4	6.8	8.0	2.4	2.6
3:1 *S:R*-Me	"	**16b**	8.1	5.8	5.2	6.2	7.0	-2.2	2.1
-	Oxy-furanyl	**15c**	8.6	6.9	6.6	7.6	8.0	1.8	2.3
4:1 *S:R*-Me	"	**16c**	7.9	5.4	5.4	7.1	6.7	-2.9	1.9

Table 1. Mean pIC_{50} values for $\alpha_v\beta_6$, $\alpha_v\beta_1$, $\alpha_v\beta_3$, $\alpha_v\beta_5$ and $\alpha_v\beta_8$ integrins in cell adhesion assays, calculated logP and measured chromatographic LogD at pH 7.4. Number of assay repeats, assay range and standard deviations are provided in the Supporting Information. "nt" means not tested. clogP values were calculated using Daylight.

Quaternary ammonium salts are potent $\alpha_v\beta_6$ inhibitors All the methyl betaines (**7**, **8**, **16a**, **16b** and **16c**) are potent inhibitors of $\alpha_v\beta_6$ with pIC_{50}'s of at least of 7.9. The most active compounds are the two isomeric betaines **7** and **8**. Given their high potencies both were also tested in the more sensitive $\alpha_v\beta_6$ radioligand binding[27] with **6**, **7** and **8** having pKi's of 10.4,[15] 9.97 (n=4)

and 9.76 (n=4) respectively. The similar binding affinity of **7** and **8** for the $\alpha_v\beta_6$ integrin is striking considering the differences in the spacial arrangement of the pyrrolidine in the two isomers (see later). The ethyl betaine **14** is less potent with an $\alpha_v\beta_6$ pIC_{50} of 7.4 presumably due to the space available in the binding site to accommodate the increased size of an ethyl group over a methyl group as in **7**.

Quaternary ammonium salts are only weak inhibitors of $\alpha_v\beta_1$, $\alpha_v\beta_3$, $\alpha_v\beta_5$ and $\alpha_v\beta_8$ and are thus highly selective for $\alpha_v\beta_6$ In general and based on the cell adhesion assay data, the quaternary ammonium salts are only moderate to weak inhibitors of $\alpha_v\beta_1$ (pIC_{50} range of 5.4-6.2), $\alpha_v\beta_3$ (pIC_{50} range of <5.0-5.3), $\alpha_v\beta_5$ (pIC_{50} range of <5.0-7.1) and $\alpha_v\beta_8$ (pIC_{50} range of 5.9-7.2) (see Table 1). As expected,[10] the compounds are slightly more potent against $\alpha_v\beta_8$ compared with $\alpha_v\beta_5$ and $\alpha_v\beta_3$ where very little activity is observed. Although this is a limited data set, as expected[10] the $\alpha_v\beta_6$ and $\alpha_v\beta_8$ cell adhesion data correlate ($r^2 = 0.81$) as do the $\alpha_v\beta_3$ and $\alpha_v\beta_5$ ($r^2 = 0.70$) whereas the r^2 values for $\alpha_v\beta_6$ and the other integrins are much poorer (see the Supporting Information for a table of r^2 values).

7 and 8 are particularly selective for $\alpha_v\beta_6$ The clinical compound **6** is a highly potent and selective $\alpha_v\beta_6$ inhibitor but its methyl quaternary salts **7** and **8** are even more selective (see Figure 7 and Table 2). Based on the workhorse cell adhesion data (Fig. 7 left-hand panel and Figure 8), both isomers are at between 1.2 – 3.4 log units selective for $\alpha_v\beta_6$ and compared with **6**. However, a more accurate reflection of the true selectivity is determined from radioligand binding assays.[27] Thus as detailed above, the $\alpha_v\beta_6$ pKi values for **7** and **8** were determined and the pKi values for the other α_v integrins can be estimated as previously described (Table 2).[10]

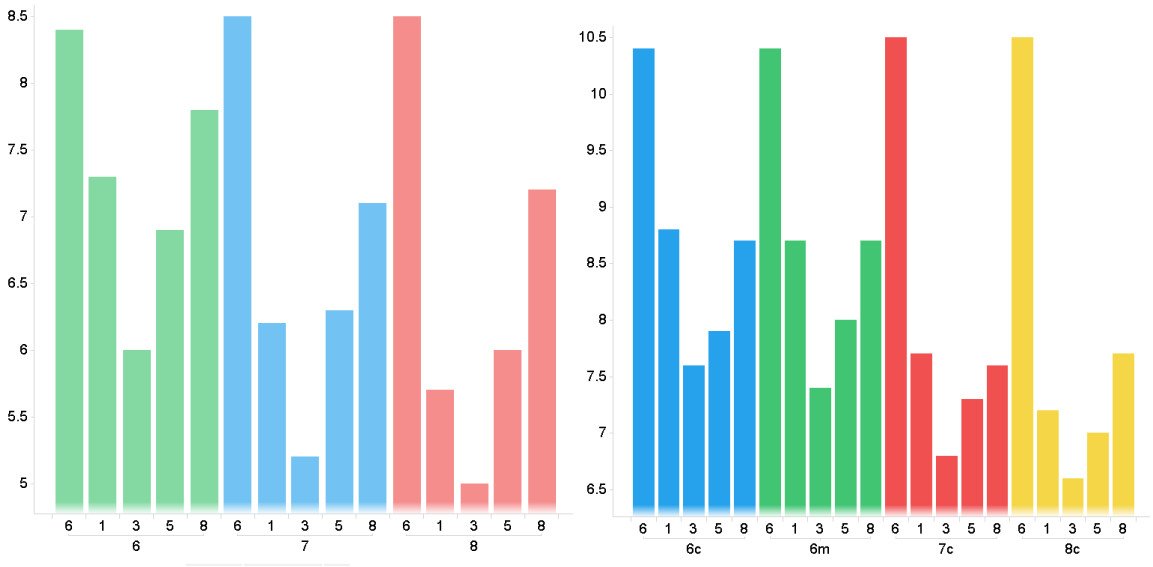

Figure 7. In both graphs on the *x*-axes and directly underneath the bars, $\alpha_v\beta_6$, $\alpha_v\beta_1$, $\alpha_v\beta_3$, $\alpha_v\beta_5$ and $\alpha_v\beta_8$ are labelled as 6, 1, 3, 5 and 8 respectively. **Left-hand panel**. α_v integrin *cell adhesion* pIC_{50} values (*y*-axis) for the parent **6** and its related *R*- and *S*-quaternary methyl ammonium salt isomers **7** and **8** respectively. Note that the first of each colored bars is higher than the other bars of the same color indicating the selectivity for $\alpha_v\beta_6$. Note also that **7** and **8** are comparatively more selective for $\alpha_v\beta_6$ over the other α_v integrins than **6**. **Right-hand panel**. Measured and calculated α_v integrin *radioligand binding* pKi's values (*y* axis) for the parent **6** and its related *R*- and *S*-quaternary methyl ammonium salt isomers **7** and **8** respectively. "**6**c" refers to values calculated from the cell adhesion data and "**6**m" refers to measured pKi values.

Pyrrol-idine subst^n	**Aryl subst^n**	**Cmpd**	**$\alpha_v\beta_6$ pKi**	**$\alpha_v\beta_1$ pKi**	**Fold 6/1**	**$\alpha_v\beta_3$ pKi**	**Fold 6/3**	**$\alpha_v\beta_5$ pKi**	**Fold 6/5**	**$\alpha_v\beta_8$ pKi**	**Fold 6/8**

-	dimethyl pyrazolo	**6**	10.4 (10.4)	8.7 (8.8)	50 (40)	7.4 (7.6)	1,000 (450)	8.0 (7.9)	250 (300)	8.7 (8.7)	50 (50)
S-Me	"	**7**	9.97 (10.5)	(7.7)	(200) -	(6.8)	(1,600) -	(7.3)	(500) -	(7.6)	(250) -
R-Me	"	**8**	9.76 (10.5)	(7.2)	(400) -	(6.6)	(1,600) -	(7.0)	(600)	(7.7)	(100)

Table 2. Measured and estimated (in brackets) pKi values for **6**, **7** and **8** alongside fold selectivity for $\alpha_v\beta_6$. Where no measured values are available, the differences shown are those from the measured $\alpha_v\beta_6$ value and the estimated $\alpha_v\beta_x$ value. Estimated pKi values were calculated by adding the following log shifts to the measured cell adhesion values: $\alpha_v\beta_1$ (+1.5) $\alpha_v\beta_3$ (+1.6), $\alpha_v\beta_5$ (+1.0), $\alpha_v\beta_6$ (+2.0), $\alpha_v\beta_8$ (+0.5) (see reference 10).

The log differences for the methyl quaternary salts **7** and **8** vary from 1.6 - 3.2 log units in the radioligand binding assays and highlights the selectivity for $\alpha_v\beta_6$ over the other α_v integrins (Fig. 7, right-hand panel and Fig. 8). In summary, **7** and **8** have 10-1,000 fold selectivity based on cell adhesion data for $\alpha_v\beta_6$ over the other α_v integrins with the true selectivity more likely to be at least 100-1,000 fold based on the radioligand binding data. **7** also has minimal activity against $\alpha5\beta1$ (pIC_{50} 5.1).[15] To the best of our knowledge these represent the most potent and selective small molecule $\alpha_v\beta_6$ inhibitors known.

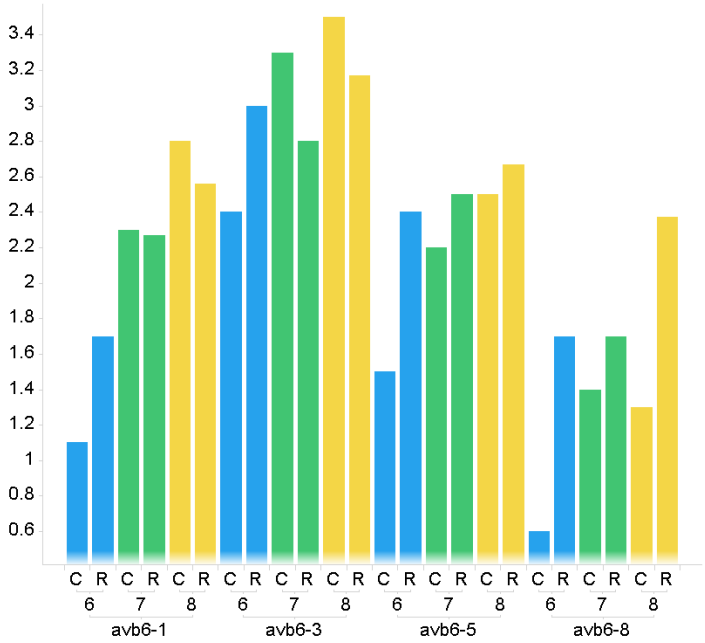

Figure 8 Graph showing the log selectivity differences *(y*-axis) for $\alpha_v\beta_6$ for each of the other α_v integrins (*x*-axis) of **6**, **7** and **8** from measured cell adhesion data and measured and estimated[10] radio ligand binding data. "C" and "R" refer to cell adhesion and radio ligand binding assays respectively. Thus "avb6-1" is the $\alpha_v\beta_6$ cell adhesion/radioligand binding value minus the $\alpha_v\beta_1$ cell adhesion/radioligand binding value. The definitions of "avb6-3", "avb6-5", "avb8-6" follow similarly.

While quaternary ammonium salts are potent $\alpha_v\beta_6$ inhibitors they are less potent than their non-quaternized parents Comparison of the $\alpha_v\beta_6$ cell adhesion data for the quaternary ammonium salts with the their respective parents shows that while they are still potent inhibitors, they are all less potent with the exception of **7** and **8** in comparison with **6** (Figure 9). However, these two are less potent based on the radioligand binding pKi values (see earlier). The reduction in inhibitory activity for the quaternary compounds over their respective parents is also seen with the other α_v integrins albeit with the absolute potencies being considerably lower (see Table 1 and Figure 10).

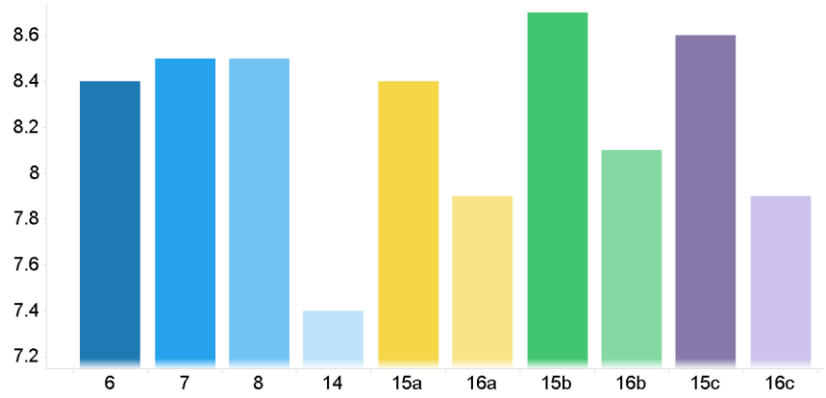

Figure 9. Plot of $\alpha_v\beta_6$ activity for the parent unquaternized compound (darkest shade) and the corresponding quaternary alkyl ammonium salts (same color but lighter shades) showing that the parents are usually more potent (except for **6**, **7** and **8** although see text).

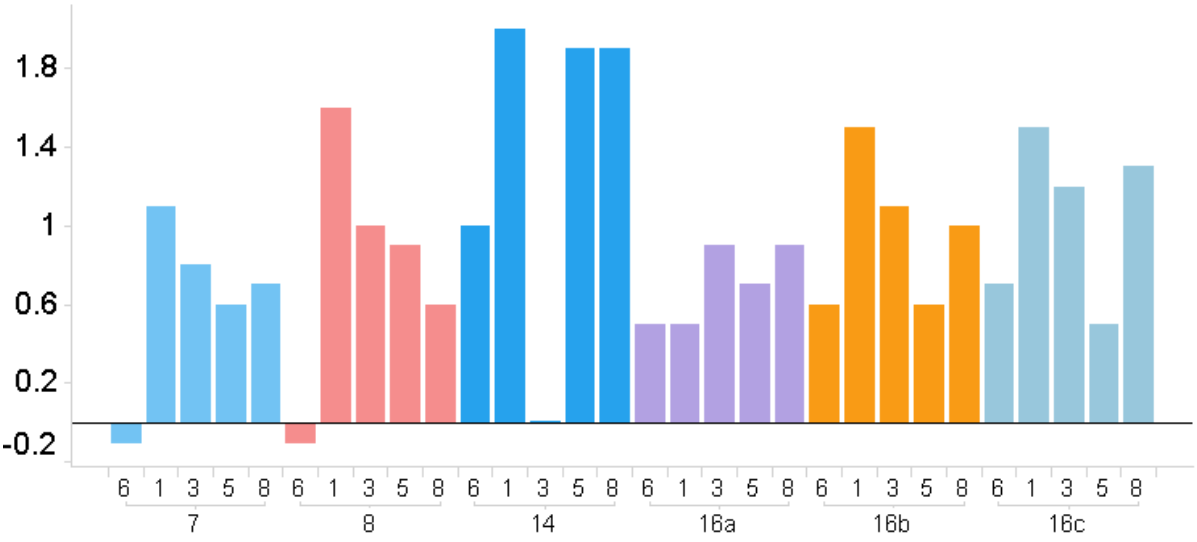

Figure 10. Plot showing the effect of quaternization on $\alpha_v\beta_6$ potency and selectivity. The *y*-axis shows the log unit difference in α_v cell adhesion pIC_{50} values between the parent pyrrolidine and the corresponding quaternary salt. On the *x*-axis, 6, 1, 3, 5 and 8 refers to $\alpha_v\beta_6$, $\alpha_v\beta_1$, $\alpha_v\beta_3$, $\alpha_v\beta_5$ and $\alpha_v\beta_8$ respectively. Same colored bars refer to the same compound also shown on the *x*-axis. Note compounds **7** and **8** maintain $\alpha_v\beta_6$ potency (in the cell adhesion

assay) compared to the parent pyrrolidine whereas the other compounds do not. **14** was not tested against $\alpha_v\beta_3$ so no bar is present.

Physicochemical profiles

The calculated logP (clogP) (Daylight) and measured chromatographic logD at pH 7.4 (chromlog$D_{7.4}$) (Table 1) are worth comment. All the methyl quaternary salt betaines **7**, **8** and **16a-c** have clogP values 4.6-4.7 log units lower than their respective parents presumably due to the software treating the pyrrolidine nitrogen as being positively charged in the betaines but not in the parents. In the case of the ethyl betaine **14**, the drop in clogP was 4.2 log units, accounting for the extra methylene. In fact, logP and logD (at various pH's) lipophilicity calculations for these compounds vary widely reflecting the complex protonation states and conformations at various pH's (see Supporting Information). In contrast, the measured chromlog$D_{7.4}$ values of the betaines are remarkably high and between 1.8 and 2.8 and are only lower by 0.3-0.5 log units in comparison to the chromlog$D_{7.4}$ values for their respective parents except in the case of **14** where there is no difference at all. This observation is attributed to the ionic charges being partially shielded as result of the conformations of the parents and the betaines as described above in the chromlog$D_{7.4}$ experiments. Chromlog$D_{7.4}$ values in this range usually show some level of permeability but in fact the permeability of the quaternized compounds is minimal (data not shown) consistent with these compounds being completely ionized. The relationship between ionization state, pH, conformation, lipophilicity, permeability and assay format for this series of compounds is inter-related and complex and will be described in detail elsewhere.

Given their structures, the aqueous kinetic solubility (CLND – chemiluminescence by nitrogen detection) of these quaternary ammonium salts is high (data not shown except for **7** *vide infra*).

Docking studies

Compound binding poses for **7** and **8** were generated by docking into the $\alpha_v\beta_6$ X-ray crystal structure (PDB code:4UM9[28]) or the $\alpha_v\beta3$ X-ray crystal structure (PDB code: 1L5G[29]) using Glide[30,31,32] (Schrödinger) (Figure 11). Both compounds exhibit bidentate H-bonds between the 1,8-tetrahydronaphthyridine and αv-Asp218. In the β-subunit, the carboxylic acid motif is coordinated with a magnesium ion (cyan sphere) in the metal ion dependent adhesion site (MIDAS) and forms H-bonds with Ala126 and Asn218. While there is some compound variation in the linking alkyl chain and the pyrrolidine ring position, the pyrrolidine *N* in both cases can form electrostatic interactions with Thr221. The *meta*-substituted aryl group location is consistent and in proximity to the specificity determining loop (SDL), forming Van der Waals interactions with Ala126, Ser182, Ile183 and Ala217 side-chains.

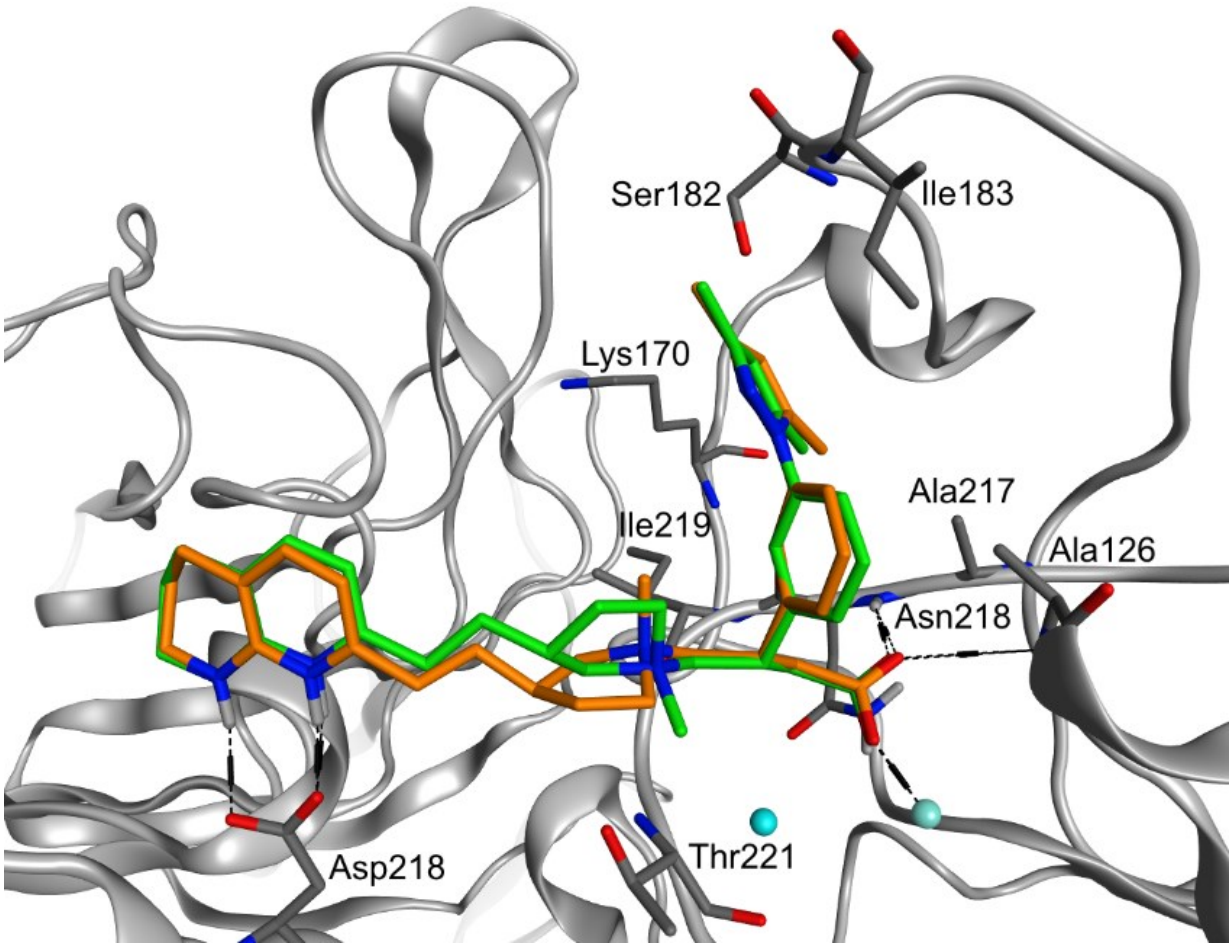

Figure 11. Predicted binding modes of **7** (green) and **8** (orange) in an $\alpha_v\beta_6$ X-ray crystal structure (PDB code:4UM9). (Note the perspective partially masks the carbons either side of the benzylic carbon for both isomers). See text for commentary.

7 was also docked into $\alpha_v\beta_3$ (Figure 12) with *H*-bonds between the 1,8-tetrahydronaphthyridine and αv-Asp218. In the β-subunit, the acid coordinates with a manganese ion (cyan sphere) of the MIDAS and forms an *H*-bond with Asn218. Due to the salt-bridge between Asp179 and Arg214 and hence a smaller β-subunit binding site size, the *meta*-substituted dimethylpyrazole ring on the aryl group is directed away from the $\alpha_v\beta_3$ SDL, forming Van der Waals interactions with the Tyr122 side-chain. This clearly contrasts with the excellent complementarity of the

dimethylpyrazolo group in the SDL for $\alpha_v\beta_6$ and provides partial explanation for the observed loss in affinity.

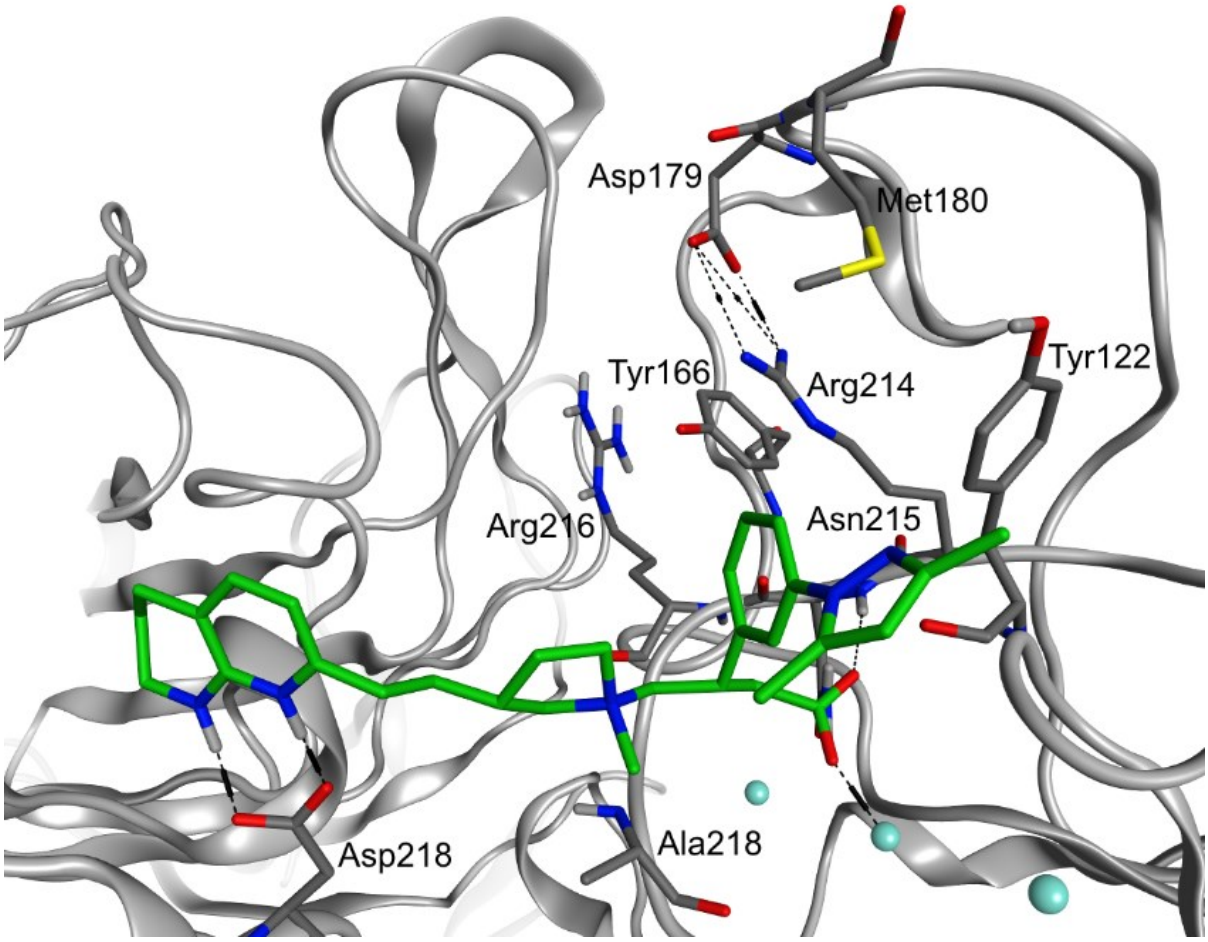

Figure 12. Docked pose of **7** (cyan) in an $\alpha_v\beta_3$ X-ray crystal structure (PDB code:1L5G).

Broader profiling of 7

Given the high potency and selectivity of **7**, we continued to evaluate it both as a tool molecule for target validation studies but also as a potential therapeutic for treating IPF. The impact of the permanently ionised state of **7** on its physicochemical, biological and pharmacokinetic

properties was further investigated to evaluate its suitability to the inhaled route of administration.

Solubility and pKa's The measured solubility of **7** by CLND is comparable to **6** (> 1 mg/mL and > 0.5 mg/mL respectively) with the thermodynamic solubility likely to be mg/mL. The tetrahydronaphthyridine and carboxylic acid groups have measured pK_a's of 7.6 and 4.0 respectively.

hERG profile The betaine **7** was assessed for cardiovascular safety in the high throughput IonWorks Barracuda Automated Patch Clamp hERG channel assay[33] and was found to have no activity ($pIC_{50} < 4.3$, n = 5).

Cross-screening Against a panel of 34 cross screens covering a range of enzymes, receptors and ion channels, **7** has minimal activity with no pXC_{50} of above 4.8 (data not shown).

In vitro DMPK studies. A significant reduction in permeability – measured on artificial membranes – is observed for the quaternary ammonium salt **7** (<8 nm/s) compared to the non ionized / non methylated version **6** (89 nm/s), potentially reducing its intra-cellular penetration although this would not affect interaction with its primary extracellular target. Comparative *in vitro* metabolic stability data for **6** and **7** in cryopreserved rat hepatocytes suggest reduced turnover for the latter (9.45 vs 1.22 mL/min/g liver respectively). However, this difference was not reflected in *in vivo* clearance (see next section) indicating either an alternative mechanism of elimination for the ionized **7** or reduced hepatocyte uptake under the experimental conditions of the *in vitro* assay. In human hepatocytes, both **6** and **7** were relatively stable *in vitro* (< 0.86 and < 0.45 mL/min/g liver respectively).

Another property affected by the ionization of the quaternary ammonium salt in **7** is its ability to bind to cellular fraction and proteins in blood (either *via* affinity to proteins or conformational effects). Higher free fractions were generally observed for **7** (58.3% and 50.3% in rat and human blood respectively) compared to **6** (29.4% and 8.3% in rat and human blood

respectively). However, **6** and **7** showed comparable protein binding in human lung homogenate (free fractions of 10.8% and 9.7% respectively).

In an electrochemical experiment with **7** and glutathione (GSH) investigating the potential for pseudo P1 metabolites, the main product observed was an oxidised form of **7** (+16Da mass observed) which also bound GSH (mass observed equated to **7** + oxygen +GSH) although it was not possible to identify the structure. The inference from this experiment is that there was no evidence of **7** acting as a methylating agent nor was the side product from this - the unmethylated parent **6 -** observed.

Pharmacokinetic studies Experimental details for the PK studies *in vivo* are reported in the supplementary information section. Betaine **7** was progressed to an *in vivo* pharmacokinetic study in the rat (n=3) as a 30-min infusion by the intravenous route. The mean blood clearance was 87.6 mL/min/kg, marginally higher that previously reported for **6** under the same experimental protocol (56 mL/min/kg). However, after correction for *in vitro* blood binding, unbound blood clearance for **6** and **7** were 150 mL/min/kg and 190 mL/min/kg respectively, thus suggesting a slightly more efficient removal of the more polar compound, probably *via* a higher contribution by the renal route. Overall, a high clearance was observed for both **6** and **7**, confirming their suitability for administration by the inhaled route, where rapid removal from the systemic circulation is often considered an upside. The mean volume of distribution observed for **7** was low-moderate, at 1.1 L/kg, with a resulting half-life of 0.22h. In comparison, **6** had previously displayed a larger volume of distribution of 2.1 L/kg, in line with the expectation that a more polar, less permeable compound should result in comparatively reduced tissue penetration.

Conclusion

The stereoselective synthesis and discovery of a remarkable set of quaternary ammonium betaines exemplified by **7** is described. These compounds, and **7** in particular, are highly potent and to the best of our knowledge, the most selective $\alpha_v\beta_6$ inhibitors known. The mode of binding of **7** to $\alpha_v\beta_6$ is described along with a more details of its biological, physicochemical and pharmacokinetic profile. Compound **7** may be of value as a small molecule tool both *in vitro* and *in vivo* and its overall profile may be suitable as an inhaled medicine for IPF. Further studies around this work will be published in due course.

Experimental

TLC was performed on Merck 0.25 mm Kieselgel 60 F_{254} plates. Products were visualized under UV light and/or by staining with aqueous $KMnO_4$ solution. LCMS analysis was conducted on one of the following four systems: System A an Acquity UPLC BEH or CSH C18 column (2.1 mm × 50 mm i.d. 1.7 μm packing diameter) eluting with 10 mM NH_4HCO_3 in water adjusted to pH 10 with aqueous ammonia (solvent A), and acetonitrile (solvent B), using the following elution gradient for BEH column: 0.0 – 1.5 min 1 – 97 % B, 1.5 – 1.9 min 97% B, 1.9 – 2.0 min 97 – 1% B, and for CSH column: 0.0 – 1.5 min 3 – 95 % B, 1.5 – 1.9 min 95% B, 1.9 – 2.0 min 95 – 3% B, at a flow-rate of 1 $mLmin^{-1}$ at 40°C. The UV detection was an averaged signal from wavelength of 210 nm to 350 nm, and mass spectra were recorded on a mass spectrometer using alternate-scan electrospray positive and negative mode ionization (ES+ve and ES-ve); System B an Acquity UPLC BEH C18 column (2.1 mm × 50 mm i.d. 1.7 μm packing diameter)) eluting with 0.1% trifluoroacetic acid in water (solvent A), and 0.1% trifluoroacetic acid in MeCN (solvent B) using the following elution gradient 0.0 – 1.5 min 3 – 100% B, 1.5 – 1.9 min 100% B, 1.9 – 2.0 min 100 – 3 % B at a flow rate of 1 mL min^{-1} at 40°C; System C an Acquity UPLC BEH or CSH C18 column (2.1 mm × 50 mm i.d. 1.7 μm packing diameter) eluting with 0.1% formic acid in water (solvent

A), and 0.1 % formic acid in acetonitrile (solvent B), using the following elution gradient 0.0 – 1.5 min 3 – 100 % B, 1.5 – 1.9 min 100% B, 1.9 – 2.0 min 100 – 3% B, at a flow rate of 1 $mLmin^{-1}$ at 40°C; System D an Acquity UPLC BEH C18 column (2.1 mm × 50 mm i.d. 1.7 μm packing diameter) eluting with 0.1% formic acid in water (solvent A), and 0.1 % formic acid in acetonitrile (solvent B), using the following elution gradient 0.0 – 0.4 min 3% B, 0.4 – 3.2 min 3 – 98% B, 3.2 – 3.8 min 98% B, 3.8 – 4.2 min 98 – 3% B, 4.2 – 4.5 min, 3% B at a flow rate of 0.6 $mLmin^{-1}$ at 35°C. Column chromatography was performed on disposable, normal phase, SPE cartridges (2 g to 100 g). Mass-directed auto-preparative HPLC (MDAP) for Method A was conducted on a Xbridge C18 column (100 mm × 30 mm i.d. 5 μm packing diameter) at ambient temperature eluting with 10 mM NH_4HCO_3 in water adjusted to pH 10 with ammonia (solvent A) and acetonitrile (solvent B), using an appropriate elution gradient over 10 min at a flow rate of 40 mL min^{-1} and detecting at 210 – 350 nm at room temperature. Method B was conducted on a Sunfire C18 column (150 mm × 30 mm i.d. 5 μm packing diameter) at ambient temperature eluting with aqueous 0.1% HCO_2H solution (solvent A) and 0.1% HCO_2H solution in acetonitrile (solvent B), using an appropriate elution gradient over 10 min at a flow rate of 40 $mLmin^{-1}$ and detecting at 210 – 350 nm at room temperature. Mass spectra were recorded using electro spray positive and negative mode, alternate scans. The accurate mass measurements were performed on an Orbitrap mass spectrometer. ^1H NMR spectra were recorded at 400 (Bruker AV-400), 500 (Bruker AV-500) or 600 MHz (Bruker AVII+ 600MHz). The chemical shifts are expressed in ppm relative to tetramethylsilane.

(3*S*)-3-(3-(3,5-Dimethyl-1*H*-pyrazol-1-yl)phenyl)-4-((1*S*,3*R*)-1-methyl-3-(2-(5,6,7,8-tetrahydro-1,8-naphthyridin-2-yl)ethyl)pyrrolidin-1-ium-1-yl)butanoate (7) and (3*S*)-3-

(3-(3,5-Dimethyl-1*H*-pyrazol-1-yl)phenyl)-4-((1*R*,3*R*)-1-methyl-3-(2-(5,6,7,8-tetrahydro-1,8-naphthyridin-2-yl)ethyl)pyrrolidin-1-ium-1-yl)butanoate (8)

To a stirred solution of **6** (100 mg, 0.205 mmol) in DCM (2 mL) heated to 35°C in a sealed vial was added iodomethane (0.128 mL, 2.051 mmol), the reaction was heated to 50°C for 5 min and added to methanol (5 mL). The reaction mixture was concentrated *in vacuo* and subjected to reverse-phase chromatography on a C18 column (12 g) eluting with 10-85% MeCN (containing 0.1% ammonia) in 10 mM aq. ammonium bicarbonate over 10 CVs. The relevant fraction was concentrated in vacuo to give a mixture of **7** and **8** (79 mg, 77%) as a colourless solid. LCMS (System A) RT=0.85 min, 98%, ES+ve *m/z* 502 $(M+H)^+$; Analytical chiral HPLC for the 1*R* isomer RT=13.6 min, 11% and for the 1*S* isomer 18.8 min, 89%, on a Chiralcel OD-H column (4.6 mm × 250 mm), eluting with 20% EtOH (containing 0.2% isopropylamine)-heptane, flow-rate=1 mL/min, detecting at 215 nm. (For other spectroscopic data see below).

(3*S*)-3-(3-(3,5-Dimethyl-1*H*-pyrazol-1-yl)phenyl)-4-((1*S*,3*R*)-1-methyl-3-(2-(5,6,7,8-tetrahydro-1,8-naphthyridin-2-yl)ethyl)pyrrolidin-1-ium-1-yl)butanoate (7)

A stirred solution of (*S*)-3-(3-(3,5-dimethyl-1*H*-pyrazol-1-yl)phenyl)-4-((*R*)-3-(2-(5,6,7,8-tetrahydro-1,8-naphthyridin-2-yl)ethyl)pyrrolidin-1-yl)butanoic acid hydrochloride (**6.HCl**)[18] (non-stoichiometric salt contains 1.6 equiv. HCl; 1.00 g, 1.83 mmol) in DCM (30 mL) was added potassium carbonate (422 mg, 3.05 mmol) and iodomethane (0.954 mL, 15.3 mmol). The mixture was stirred at room temperature for 69 h and then the solvent was removed *in vacuo.* The residual solid (1.96 g) was purified by reverse-phase chromatography on a C18 column (120 g) eluting with 10-85% MeCN (containing 0.1% ammonia) in 10 mM aq. ammonium bicarbonate over 14 column volumes. The appropriate fractions were combined and concentrated *in vacuo* to give **7** (760 mg, 83%) as a yellow solid: LCMS (System A)

RT=0.83 min, 100%, ES+ve *m/z* 502 $(M+H)^+$; ^{1}H NMR (CD_3CN, 600 MHz) δ 7.46-7.42 (2H, m), 7.38-7.35 (1H, m), 7.33-7.30 (1H, m), 7.03 (1H, d, *J* 7.3 Hz), 6.28 (1H, d, *J* 7.3 Hz), 6.02 (1H, s), 5.57 (1H, br s), 4.05-3.99 (1H, m), 3.83-3.77 (1H, m), 3.75-3.65 (2H, m), 3.54 (1H, t, *J* 11 Hz), 3.42 (1H, dt, *J* 12, 8.5 Hz), 3.30 (2H, t, *J* 5.5 Hz), 3.20-3.14 (1H, m), 2.83 (3H, s), 2.64 (2H, t, *J* 6 Hz), 2.51-2.39 (3H, m), 2.34-2.29 (1H, m), 2.29 (3H, s), 2.26-2.23 (1H, m), 2.20 (3H, s), 2.20-2.14 (1H, m), 1.84-1.66 (5H, m); ^{13}C NMR (CD_3CN, 151 MHz) δ 173.2, 157.6, 156.7, 149.2, 146.1, 141.3, 140.3, 137.0, 130.3, 126.9, 124.0, 123.4, 117.9, 113.8, 111.1, 107.6, 70.7, 69.9, 65.9, 50.4, 46.3, 46.2, 41.6, 41.1, 40.6, 36.1, 35.8, 33.3, 29.1, 26.7, 21.9, 13.2, 12.4. HRMS (ESI) calc'd for $C_{30}H_{40}N_5O_2$ $(M+H)^+$ 502.3182, found 502.3192. $[\alpha]_D^{23}$ = +36 (c = 0.5, $CHCl_3$), $[\alpha]_D^{21}$ = +11° (c=1.0 in EtOH). Analytical chiral HPLC RT=17.9 min, 99.5%, on a Chiralcel OD-H column (4.6 mm × 250 mm), eluting with 20% EtOH (containing 0.2% isopropylamine)-heptane, flow-rate=1 mL/min, detecting at 215 nm.

NOE correlation is observed between the N-CH_3 singlet at 2.83 ppm and the pyrrolidine 3-H in the multiplet at 2.51-2.39 ppm confirming that both are on the same face of the pyrrolidine ring. This therefore confirms the configuration of the quaternary nitrogen stereocenter as (*S*).

Larger scale preparation of 7 using SFC purification

Seven lots of **6.HCl** (non-stoichiometric salt, 1.6 equiv. HCl; 1.00 g, 1.83 mmol) and potassium carbonate (0.330 g, 2.38 mmol) were added in seven separate vials, DCM (20 mL) was added and the vials were sealed. Iodomethane (0.15 mL, 2.4 mmol) was added via syringe to each vial and the reaction mixtures were stirred for 69 h at 20°C. The contents of the vials were combined and the solvent removed *in vacuo* at room temperature (no heating). The residue (10.3 g) was purified by SFC conducted on a Torus 2-PIC column (150 mm × 19 mm) eluting with a gradient of 15-35% MeOH (containing 0.2% v/v aq. ammonia) - CO_2 at a

pressure of 170 bar, flow-rate 68 mL/min, detecting at 220 nm at 40°C. Appropriate fractions were combined, diluted with water and then freeze-dried to give *the title compound* (4.2 g, 65%) as a white solid: LCMS (System A) RT=0.82 min, 100%, ES+ve *m/z* 502 $(M+H)^+$; ^{1}H NMR (DMSO-d_6, 600 MHz) 7.54 (1H, s), 7.45-7.41 (2H, m), 7.35-7.32 (1H, m), 7.04 (1H, d, *J* 7.3 Hz), 6.47 (1H, br s), 6.27 (1H, d, *J* 7.3 Hz), 6.07 (1H, s), 3.91 (1H, dd, *J* 13.2, 9.5 Hz), 3.80-3.75 (2H, m), 3.69 (1H, m), 3.39 (1H, t, *J* 11 Hz), 3.33-3.28 (1H, m), 3.26-3.21 (3H, m), 2.83 (3H, s), 2.60 (2H, br t, *J* 6.2 Hz), 2.45-2.33 (4H, m), 2.29 (3H, s), 2.22-2.14 (2H, m), 2.19 (3H, s), 1.76-1.68 (4H, m), 1.68-1.61 (1H, m); ^{13}C NMR (DMSO-d_6, 151 MHz) δ 172.0, 156.1, 155.6, 147.7, 144.9, 139.9, 139.1, 136.2, 129.3, 126.3, 123.3, 122.5, 112.7, 109.8, 107.1, 68.8, 68.4, 64.3, 48.8, 44.4, 40.6, 38.4, 35.1, 34.4, 32.9, 27.9, 25.9, 20.9, 13.2, 12.1.

Purity by reverse phase HPLC (column CSH C18 (100mm x 2.1 mm id 1,7um), solvent A 0.1% formic acid in water, solvent B 0.1% formic acid in MeCN, 8.5 minute gradient from 3%B to 99.9%B) showed **7** to be 99.22% pure. See SI for full details.

(*S*)-3-(3-(3,5-Dimethyl-1*H*-pyrazol-1-yl)phenyl)-4-((1*R*,3*R*)-1-methyl-3-(2-(5,6,7,8-tetrahydro-1,8-naphthyridin-2-yl)ethyl)pyrrolidin-1-ium-1-yl)butanoate (8)

Methyl (*S*)-3-(3-(3,5-dimethyl-1*H*-pyrazol-1-yl)phenyl)-4-((*R*)-3-(2-(5,6,7,8-tetrahydro-1,8-naphthyridin-2-yl)ethyl)pyrrolidin-1-yl)butanoate (**11**) (110 mg, 0.219 mmol) and potassium carbonate (36 mg, 0.26 mmol) were suspended in DCM (2 mL). Iodomethane (0.02 mL, 0.32 mmol) was added and stirred for 2 days. The solvent was removed under a stream of nitrogen at room temperature. The residue was dissolved in DMSO (2 mL) and purified by MDAP on a Xselect CSH C18 column (150 mm × 30 mm i.d. 5μm packing diameter) at ambient temperature eluting with a gradient of 50-99% 10 mM aq. ammonium bicarbonate solution – acetonitrile over 25 min, flow-rate 40 mL/min. The solvent was evaporated *in*

vacuo to give (3*R*)-1-((*S*)-2-(3-(3,5-dimethyl-1*H*-pyrazol-1-yl)phenyl)-4-methoxy-4-oxobutyl)-1-methyl-3-(2-(5,6,7,8-tetrahydro-1,8-naphthyridin-2-yl)ethyl)pyrrolidin-1-ium (**12**) (72 mg, 64%) as a 2:1 mixture of diastereomers (by NMR). LCMS (System A) RT=1.25 min, 97%, ES+ve *m/z* 516 $(M+H)^+$; ^{1}H NMR (DMSO-d_6, 400 MHz) 7.62 (1H, s), 7.52–7.48 (2H, m), 7.43–7.37 (1H, m), 7.04 (1H, d, *J* 7.3 Hz), 6.27 (1H, d, *J* 7.3 Hz), 6.17 (1H, m), 6.09 (1H, s), 4.03–3.56 (6H, m), 3.28–3.14 (5H, m), 2.88 (3H, s), 2.95–2.83 (1H, m), 2.77–2.66 (1H, m), 2.61 (2H, t, *J* 6 Hz), 2.46-2.38 (2H, m), 2.30 (3H, s), 2.28–2.20 (2H, m), 2.19 (3H, s), 1.79–1.59 (5H, m). The diastereomeric mixture of **12** (72 mg, 0.139 mmol) was dissolved in THF (1 mL) and 2M aq. LiOH (0.209 mL, 0.418 mmol) was added and stirred for 16 h. The reaction mixture was acidified to pH 4 with 2M hydrochloric acid and then the solvent removed *in vacuo*. The residue was dissolved in DMSO (1.2 mL) and purified by MDAP on a Xselect CSH C18 column (150 mm × 30 mm i.d. 5 μm packing diameter) at ambient temperature eluting with a gradient of 50-99% 10 mM aq. ammonium bicarbonate solution – acetonitrile over 25 min, flow-rate 40 mL/min. The solvent was evaporated in vacuo to give a colourless oil (39 mg) which was a 2.6:1 mixture of diastereomers (by NMR). The isomers were separated by preparative chiral HPLC on Chiralcel OD-H column (250 mm × 30 mm) eluting with 50% EtOH-heptane, flow rate=30 mL/min, detecting at 215 nm. The relevant fractions were collected and concentrated *in vacuo* to afford **8** (6 mg, 8%) as a white solid: LCMS (System A) RT=0.81 min, 100%, ES+ve *m/z* 502 $(M+H)^+$; ^{1}H NMR (DMSO-d_6, 600 MHz) 7.52–7.48 (1H, m), 7.45–7.41 (1H, m), 7.41–7.37 (1H, m), 7.32 (1H, dt, *J* 7.7, 2 Hz), 7.00 (1H, d, *J* 7.3 Hz), 6.35 (1H, s), 6.18 (1H, d, *J* 7.3 Hz), 6.06 (1H, s), 3.86–3.80 (1H, m), 3.80–3.72 (2H, m), 3.67–3.61 (1H, m), 3.64–3.56 (1H, m), 3.49–3.42 (1H, m), 3.22 (2H, br t, *J* 5.3 Hz), 2.93 (3H, s), 2.95–2.87 (1H, m), 2.58 (2H, t, *J* 6 Hz), 2.27 (3H, s), 2.30–2.26 (2H, m), 2.32–2.24 (1H, m), 2.26–2.20 (1H, m), 2.16 (3H, s), 2.20–2.12 (1H, m), 2.03 (1H, dd, *J* 4, 15.5 Hz), 1.76–1.69 (2H, m), 1.74–1.68 (1H, m), 1.70–1.57 (2H, m); ^{13}C NMR δ (DMSO-

d_6, 151 MHz) 171.2, 156.4, 155.7, 147.6, 145.6, 139.8, 139.0, 135.9, 129.3, 126.0, 123.1, 122.3, 112.4, 109.6, 107.0, 68.9, 66.8, 63.3, 50.9, 46.1, 40.6, 38.7, 35.6, 35.2, 32.9, 28.2, 25.9, 20.9, 13.2, 12.0. $[\alpha]_D^{21}$ = +2° (c=1.0 in EtOH); Anal. Chiral HPLC RT=14.2 min, 100% on a Chiralcel OD-H column (250 mm × 4.6 mm) eluting with 20% EtOH-heptane, flow-rate=1.0 mL/min, detecting at 230 nm. Evaporation of the other relevant fractions gave **7** (16 mg, 23%) as a white solid: LCMS (System A) RT=0.82 min, 100%, ES+ve *m/z* 502 $(M+H)^+$. Anal. Chiral HPLC RT=16.7 min, 98.2% on a Chiralcel OD-H column (250 mm × 4.6 mm) eluting with 20% EtOH-heptane, flow-rate=1.0 mL/min, detecting at 230 nm.

(1*S*,3*R*)-1-((*S*)-3-Carboxy-2-(3-(3,5-dimethyl-1*H*-pyrazol-1-yl)phenyl)propyl)-1-methyl-3-(2-(5,6,7,8-tetrahydro-1,8-naphthyridin-2-yl)ethyl)pyrrolidin-1-ium iodide (9)

A mixture of **6.HCl** (non-stoichiometric salt, 1.6 equiv. HCl; 1.00 g, 1.83 mmol) and potassium carbonate (422 mg, 3.05 mmol) were combined in DCM (20 mL) in a vial and sealed. Iodomethane (0.95 mL, 15.19 mmol) was added via syringe and the reaction stirred for 68 h. The reaction mixture was filtered through a bed of Celite®, washing with DCM (20 mL). The filtrate and washings were diluted with methanol (10 mL) and the solvent removed *in vacuo*. The residue was dissolved in DCM (4 mL) and purified by chromatography on a silica cartridge (80 g), eluting with 0-20% methanol in DCM over 50 min. Fractions were collected and the solvent removed *in vacuo* to give **9** (285 mg, 25%) as a white solid: LCMS (System A) RT=0.83 min, 100%, ES+ve *m/z* 502 $(M+H)^+$; ^{1}H NMR δ (DMSO-d_6, 600 MHz) 7.61 (1H, s), 7.55-7.44 (3H, m), 7.43-7.38 (1H, m), 7.18 (1H, d, *J* 7.15 Hz), 6.35 (1H, d, *J* 7.15 Hz), 6.09 (1H, s) 3.98 (1H, dd, *J* 13, 9.6 Hz) 3.79-3.67 (4H, m), 3.41-3.24 (3H, m), 2.83 (3H, s), 2.70 (1H, dd, *J* 17, 8.5 Hz), 2.64 (2H, t, *J* 6 Hz), 2.48-2.40 (3H, m), 2.31 (3H, s), 2.27-2.21 (1H, m), 2.25 (1H, m, *J* 13, 8 Hz), 2.19 (3H, s), 2.19 (1H, d, *J* 5 Hz), 1.81-1.67 (5H, m); ^{13}C NMR δ (DMSO-d_6, 151 MHz) 173.7, 148.3, 143.9, 140.4, 139.7, 137.8, 130.0,

126.9, 124.0, 123.4, 110.2, 110.0, 107.6, 68.7, 68.0, 65.5, 55.3, 49.7, 41.8, 40.9, 37.9, 35.3, 34.1, 28.6, 26.1, 20.9, 13.7, 12.6. Ion chromatography for iodide content. Found: I, 20.5%; $C_{30}H_{40}N_5O_2^+I^-$ requires I, 20.2%.

(1*S*,3*R*)-1-((*S*)-3-carboxy-2-(3-(3,5-dimethyl-1*H*-pyrazol-1-yl)phenyl)propyl)-1-methyl-3-(2-(5,6,7,8-tetrahydro-1,8-naphthyridin-2-yl)ethyl)pyrrolidin-1-ium chloride, hydrochloride (10)

A solution of **7** (50 mg, 0.10 mmol) in dichloromethane (1 mL) was treated with a solution of HCl in dioxane (4M, 25 μL, 0.1 mmol), stirred for 1 h and then the solvent was removed *in vacuo*. The residue was dissolved in diethyl ether (5 mL) and the solvent was removed under a flow of nitrogen and dried in vacuo at 40°C for 1 h. The residue was then further dissolved in diethyl ether (5 mL) and the solvent removed under a flow of nitrogen. The residue was then dissolved in chloroform (5 mL) and the solvent removed under a flow of nitrogen, dried in vacuo at 40°C for 1 h to give **10** (44 mg, 77%) as a white glass: LCMS (System A) RT=0.83 min, 100%, ES+ve *m/z* 502 $(M+H)^+$; ^{1}H NMR δ (DMSO-d_6, 600 MHz) 14.51 (1H, br s), 12.38 (1H, s), 8.10 (1H, br s), 7.63-7.61 (1H, m), 7.62-7.59 (1H, m), 7.53-7.49 (1H, m), 7.51-7.46 (1H, m), 7.41-7.38 (1H, m), 6.61 (1H, d, *J* 7.3 Hz), 6.08 (1H, s), 4.02-3.96 (1H, m), 3.93-3.87 (1H, m), 3.77-3.73 (1H, m), 3.78-3.72 (1H, m), 3.44-3.41 (2H, m), 3.30-3.26 (1H, m), 3.26-3.19 (2H, m), 2.90 (3H, s), 2.84-2.78 (1H, m), 2.73 (2H, br t, *J* 6 Hz), 2.69-2.64 (2H, m), 2.65-2.59 (1H, m), 2.48-2.42 (1H, m), 2.30 (3H, s), 2.24-2.18 (1H, m), 2.18 (3H, s), 1.84-1.78 (2H, m), 1.84-1.77 (2H, m), 1.75-1.70 (1H, m); ^{13}C NMR δ (DMSO-d_6, 151 MHz) 171.7, 151.2, 147.7, 146.9, 142.6, 140.9, 139.8, 139.2, 129.4, 126.5, 123.7, 123.0, 118.9, 110.0, 107.1, 68.5, 68.2, 63.9, 48.1, 40.5, 40.3, 37.0, 33.5, 32.0, 30.2, 27.2, 24.7, 18.9, 13.2, 12.1.

(3*S*)-3-(3-(3,5-Dimethyl-1*H*-pyrazol-1-yl)phenyl)-4-((1*S*,3*R*)-1-ethyl-3-(2-(5,6,7,8-tetrahydro-1,8-naphthyridin-2-yl)ethyl)pyrrolidin-1-ium-1-yl)butanoate (14)

A solution of **6** (1.00 g, 2.05 mmol) in DCM (5 mL) was treated with iodoethane (0.824 mL, 10.3 mmol) and the reaction mixture was stirred at room temperature for 48 h in a sealed vessel. After 24 h more iodoethane (2 equiv.) was added and the mixture heated to 45°C for 4 h, and then stirred at room temperature for a further 20 h. The reaction reached equilibrium and an aliquot of the reaction mixture (100 mg) was purified by MDAP eluting with a gradient of MeCN-aq. 10 mM ammonium bicarbonate containing ammonia to pH 10, over 25 min; the product was isolated and re-purified by MDAP using a gradient of MeCN – aq. 0.1% formic acid, over 25 min. The appropriate fractions were evaporated to give **14** as a white solid (10.3 mg, 1% based on the100 mg aliquot purified, extrapolated to 10% if all crude product were purified): LCMS (System B formic) RT=0.49 min, 100%, ES+ve *m/z* 516 $(M+H)^+$; ^{1}H NMR (DMSO-d_6, 600 MHz) 7.61 (1H, t, *J* 1.5 Hz), 7.52-7.49 (1H, m), 7.47 (1H, t, *J* 7.5 Hz), 7.37 (1H, dt, *J* 7.5, 1.5 Hz), 7.09 (1H, d, *J* 7.3 Hz), 6.83 (1H, br s), 6.30 (1H, d, *J* 7.3 Hz), 6.07 (1H, s), 3.85 (1H, dd, *J* 14, 10 Hz), 3.78 (1H, dd, *J* 12, 8 Hz), 3.66 (2H, d, *J* 12.5 Hz,), 3.53 (1H, t, *J* 11 Hz), 3.33-3.27 (1H, m), 3.26-3.21 (3H, m), 3.19-3.09 (2H, m), 2.61 (2H, t, *J* 6 Hz), 2.60-2.56 (1H, m), 2.48-2.41 (2H, m), 2.40-2.31 (2H, m), 2.29 (3H, s), 2.18 (3H, s), 2.12 (1H, dq, *J* 14, 7 Hz), 1.77-1.73 (2H, m), 1.73-1.68 (2H, m), 1.68-1.59 (1H, m), 0.96 (3H, t, *J* 7 Hz); ^{13}C NMR (DMSO-d_6, 151 MHz) 173.0, 155.4, 155.3, 147.8, 143.8, 139.9, 139.2, 136.6, 129.5, 126.4, 123.5, 122.9, 113.3, 109.8, 107.1, 66.3, 64.3, 62.5, 54.4, 42.6, 40.5, 37.4, 34.7, 34.7, 33.0, 28.4, 25.8, 20.7, 13.2, 12.1, 7.8.

NOE correlation is observed between the N-CH_2CH$_3$ methylene protons at 3.33-3.27 (m) and 3.19-3.09 (m) ppm and the pyrrolidine 3-H in the multiplet at 2.40-2.31 ppm confirming that both are on the same face of the pyrrolidine ring. This therefore confirms the configuration of the quaternary nitrogen stereocenter as (*S*).

(*S*)-4-((1*S*,3*R*)-1-Methyl-3-(2-(5,6,7,8-tetrahydro-1,8-naphthyridin-2-yl)ethyl)pyrrolidin-1-ium-1-yl)-3-(3-morpholinophenyl)butanoate (16a) (and (17a))

(*S*)-3-(3-Morpholinophenyl)-4-((*R*)-3-(2-(5,6,7,8-tetrahydro-1,8-naphthyridin-2-yl)ethyl)pyrrolidin-1-yl)butanoic acid (**15a**) (100 mg, 0.209 mmol) was suspended in DCM (2 mL) in a vial and sealed. Iodomethane (0.105 mL, 1.671 mmol) was added to the mixture via syringe and stirred for 68 h. The reaction mixture was filtered through a small bed of celite, and washed with DCM (10 mL). The filtrate was concentrated under a stream of nitrogen without heating. The residue was dissolved in DMSO (1 mL) and purified by MDAP on XSelect CSH column using acetonitrile – aq. ammonium bicarbonate solution. The solvent was evaporated in vacuo to give **16a** and **17a** as a 5:1 mixture of diastereomers (by NMR) (15 mg, 15%): LMCS (System A) RT=0.76 min, 100%, ES+ve *m/z* 493 $(M+H)^+$; 1H NMR (CD_3CN, 500 MHz) 7.26 (1H, t, *J* 8 Hz), 7.14 (1H, d, *J* 7.3 Hz, 1H), 6.95 (t, *J* 2 Hz), 6.87-6.82 (2H, m), 6.35 (1H, d, *J* 7.3 Hz), 3.90-3.87 (1H, m), 3.82-3.79 (4H, m), 3.82 (1H, s), 3.78-3.73 (1H, m), 3.62-3.58 (1H, m), 3.60 (1H, br dd, *J* 8, 12 Hz), 3.48-3.41 (1H, m), 3.38-3.34 (2H, m), 3.26-3.20 (1H, m), 3.18-3.15 (4H, m), 2.81 (3H, s), 2.69 (2H, br t, *J* 6.3 Hz), 2.54-2.49 (1H, m), 2.53-2.48 (2H, m), 2.43-2.36 (1H, m), 2.32-2.28 (1H, m), 2.27-2.22 (1H, m), 1.88-1.84 (2H, m), 1.82-1.76 (2H, m), 1.81-1.74 (1H, m); ^{13}C NMR (CD_3CN, 126 MHz) 175.7, 166.3, 156.4, 153.2, 145.5, 138.4, 130.7, 119.3, 118.8, 115.1, 114.9, 111.6, 70.8, 69.5, 67.4, 66.6, 51.6, 50.3, 45.5, 42.1, 41.3, 36.4, 35.9, 34.8, 30.1, 27.1, 22.1.

NOE correlation is observed between the N-CH_3 singlet at 2.81 ppm and the pyrrolidine 3-H in the multiplet at 2.54-2.49 ppm confirming that both are on the same face of the pyrrolidine ring. This therefore confirms the configuration of the quaternary nitrogen stereocenter as (*S*).

(*S*)-3-(3-(5-Methyl-1*H*-pyrazol-1-yl)phenyl)-4-((1*S*,3*R*)-1-methyl-3-(2-(5,6,7,8-tetrahydro-1,8-naphthyridin-2-yl)ethyl)pyrrolidin-1-ium-1-yl)butanoate (16b) (and 17b))

A suspension of (*S*)-3-(3-(5-methyl-1*H*-pyrazol-1-yl)phenyl)-4-((*R*)-3-(2-(5,6,7,8-tetrahydro-1,8-naphthyridin-2-yl)ethyl)pyrrolidin-1-yl)butanoic acid, hydrochloride (**15b.HCl**) (30 mg, 0.059 mmol) and potassium carbonate (11 mg, 0.080 mmol) in DCM (1 mL) was treated with iodomethane (5 µL, 0.080 mmol), the reaction mixture was stirred for 17 h in a sealed vial and then for a further 24 h. The mixture was concentrated and the residue was dissolved in DMSO (0.6 mL) and purified by MDAP on XSelect CSH column using acetonitrile – aq. ammonium bicarbonate solution. Appropriate fractions were evaporated in vacuo to give **16b** and **17b** (10 mg, 35%) as a mixture of diastereomers in the ratio of 3:1 respectively (by NMR): LCMS (System A) RT=0.81 min, 100%, ES+ve *m/z* 488 $(M+H)^+$; ^{1}H NMR (DMSO-d_6, 600 MHz) 7.61 (1H, s), 7.55 (1H, br d, *J* 1.5 Hz), 7.52-7.47 (2H, m), 7.41-7.38 (1H, m), 7.07 (1H, d, *J* 7.3 Hz), 6.28 (1H, s), 3.95 (2H, dd, *J* 13.5, 10 Hz), 3.80-3.72 (4H, m), 3.43 (1H, t, *J* 10.6 Hz), 3.35-3.29 (1H, m), 3.27-3.20 (3H, m), 2.84 (3H, s), 2.62 (2H, t, *J* 6 Hz), 2.46-2.36 (3H, m), 2.34 (3H, s), 2.27-2.17 (1H, m), 1.77-1.65 (4H, m).

For the major isomer, NOE correlation is observed between the N-CH_3 singlet at 2.84 ppm and the pyrrolidine 3-H in the multiplet at 2.44 ppm confirming that both are on the same face of the pyrrolidine ring. This therefore confirms the configuration of the quaternary nitrogen stereocenter as (*S*). These enhancements are not observed in the minor component, which is consistent with the minor isomer having the (*R*) configuration at the nitrogen stereocenter.

(*S*)-4-((1*S*,3*R*)-1-Methyl-3-(2-(5,6,7,8-tetrahydro-1,8-naphthyridin-2-yl)ethyl)pyrrolidin-1-ium-1-yl)-3-(3-(((*R*)-tetrahydrofuran-3-yl)oxy)phenyl)butanoate (16c) (and 17c))

A suspension of (*S*)-4-((*R*)-3-(2-(5,6,7,8-tetrahydro-1,8-naphthyridin-2-yl)ethyl)pyrrolidin-1-yl)-3-(3-(((*R*)-tetrahydrofuran-3-yl)oxy)phenyl)butanoic acid (**15c**) (30 mg, 0.063 mmol) and potassium carbonate (11 mg, 0.080 mmol) in DCM (1 mL) was treated with iodomethane (7 μL, 0.1 mmol) and stirred for 41 h. The reaction mixture was concentrated and the residue was dissolved in DMSO (0.6 mL) and purified by MDAP on XSelect samples column using acetonitrile – aq. ammonium bicarbonate solution. Appropriate fractions were evaporated in vacuo to give **16c** and **17c** as a mixture of diastereomers in the ratio of 4:1 respectively (by NMR) (3.4 mg, 11%) as a colourless gum: LCMS (System A) RT=0.79 min, 100%, ES+ve *m/z* 494 $(M+H)^+$; ^{1}H NMR (DMSO-d_6, 600 MHz) 7.25 (1H, t, *J* 8 Hz), 7.07 (1H, d, *J* 7.3 Hz), 7.03-6.98 (2H, m), 6.78 (1H, br d, *J* 8 Hz), 6.68-6.57 (1H, br), 6.28 (1H, d, *J* 7.3 Hz), 5.03 (1H, m), 3.92-3.79 (4H, m), 3.78-3.67 (4H, m), 3.62-3.45 (3H, m), 3.40 (1H, t, *J* 11 Hz), 3.32-3.27 (1H, m), 3.26-3.22 (2H, m), 2.82 (3H, s), 2.60 (2H, t, *J* 6 Hz), 2.45-2.37 (3H, m), 2.28-2.15 (3H, m), 1.98-1.92 (1H, m), 1.77-1.62 (4H, m).

For the major isomer, ROESY and 1D-ROESY enhancements are observed between the N-CH_3 singlet at 2.82 ppm and the pyrrolidine 3-H in the multiplet at 2.43 ppm confirming that both are on the same face of the pyrrolidine ring. This therefore confirms the configuration of the quaternary nitrogen stereocenter as (*S*). These enhancements are not observed in the minor component, which is consistent with the minor isomer having the (*R*) configuration at the nitrogen stereocenter.

Quantum chemical calculations Quantum chemical calculations were performed on compounds **7**, **8** and the anionic and neutral forms of **6**. The conformer generation was performed using Macromodel,[21] with the OPLS3 forcefield[34] and the GB/SA solvation model[35] (PCM is the polarizable continuum model which is an implicit solvation model and used mostly

in quantum chemistry. GB/SA is the Generalized Born/Solvent Accessible Surface model which is an implicit solvation model.)

The number of conformers generated were between 60-220. Quantum chemical calculations were performed on these conformations using Gaussian 16 code[22] using an *a posteriori* dispersion corrected B3LYP functional[23](B3LYP-D3) using a PCM solvation model with CH_2Cl_2,[24] and the 6-31+G** basis set.[25] The minimum character of the stationary points obtained by full geometry optimizations on all the structures were confirmed by frequency calculations. The conformations with the lowest calculated solution phase energy were then analysed.

Pharmacokinetic Studies. All animal studies were ethically reviewed and carried out in accordance with Animals (Scientific Procedures) Act 1986 and the GSK Policy on the Care, Welfare and Treatment of Animals. Comprehensive experimental details for the studies described here are provided in the Supporting Information.

Acknowledgements. We thank Eric Hortense for the analytical HPLC on chiral stationary phase, Nigel Deeks for the glutathione experiment with **7**, Steve Jackson for the separation of diastereomers by preparative chiral HPLC, Elliot Stephens for technical support, Neil Fazackerley for Spotfire support and Jared Marklew for assisting with graphics. We thank Pan Procopiou for preparing the first draft of this paper.

Supporting Information. The supporting information contains (1) ^{1}H-NMR spectra for compounds **7** and **8;** (2) ^{1}H-NMR of **6** at different concentrations; (3) Table of cell adhesion data, n numbers and standard deviations; (4) Table of cell adhesion value correlations; (5) Table of various lipophilicity calculations; (6) SMILES for the compounds described; (7)

DMPK Experimental section; (8) XL and modelling files and pdf file; (9) Purity of compound **7.**

AUTHOR INFORMATION

Corresponding Author

*E-mail: simon.jf.macdonald@gsk.com. Phone: (+44)1438 790495

790495. Fax: (+44)1438 768302.

ORCID

Panayiotis A. Procopiou: 0000-0001-5907-116X

Simon J. F. Macdonald: 0000-0002-4859-8246

Notes

The authors declare the following competing financial interest(s): Most of the authors are shareholders in GlaxoSmithKline.

Abbreviations used: chromlogD chromatographic logD; CLND, chemiluminescence nitrogen detection; GB/SA, generalized born/solvent accessible surface model; IPF, idiopathic pulmonary fibrosis; MDAP, mass directed HPLC automated purification; OPLS3, optimized potentials for liquid simulations 3; MeCN, acetonitrile; MIDAS, metal ion dependent adhesion site; PCM, polarizable continuum model; RGD, arginine-glycine-aspartic acid; SDL, specificity determining loop.

[1] Nanthakumar, C. B.; Hatley, R. J. D.; Lemma, S.; Gauldie, J.; Marshall, R. P.; Macdonald, S. J. F. Dissecting fibrosis: therapeutic insights from the small-molecule toolbox. *Nat. Rev. Drug Disc*. **2015**, *14*, 693-720.

[2] Richeldi, L.; Collard, H. R.; Jones, M. G. Idiopathic pulmonary fibrosis. *The Lancet* **2017**, *389*, 1941-1952.

[3] Datta, A.; Scotton, C. J.; Chambers, R. C. Novel therapeutic approaches for pulmonary fibrosis. *Br. J. Pharmac.* **2011,** *163,* 141-172.

[4] Raghu, G.; Richeldi, L. Current approaches to the management of idiopathic pulmonary fibrosis. *Respiratory Medicine* **2017**, *129*, 24-30.

[5] Mora, A.L.; Rojas, M.; Pardo, A.; Selman, M. Emerging therapies for idiopathic pulmonary fibrosis, a progressive age-related disease *Nature Reviews Drug Disc*. **2017**, *16*, 755-772.

[6] Barczyk, M.; Carracedo, S.; Gullberg, D. Integrins. *Cell Tissue Res*. **2010**, *339*, 269-280.

[7] Bandyopadhyay, A.; Raghavan, S.; Defining the role of integrin $\alpha_v\beta_6$ in cancer. *Curr. Drug Targets* **2009**, *10*, 645-652.

[8] Ley, K.; Rivera-Nieves, J.; Sandborn, W. J.; Shattil, S. Integrin-based therapeutics: biological basis, clinical use and new drugs. *Nat. Rev. Drug Disc*. **2016**, *15*, 173-183.

[9] Miller, L. M.; Pritchard, J. M.; Macdonald, S. J. F.; Jamieson, C.; Watson, A. J. B. Emergence of small-molecule non-RGD-mimetic inhibitors for RGD integrins. *J. Med. Chem.* **2016**, *60*, 3241-3251.

[10] Hatley, R. J. D.; Macdonald, S. J. F.; Slack, R. J.; Lukey, P. T. An av-RGD integrin inhibitor toolbox: drug discovery insight, challenges and opportunities. *Angew. Chem. Int. Ed*. **2017**, *57*, 3298-3321.

[11] Sheldrake, H. M.; Patterson, L. H. Strategies to inhibit tumor associated integrin receptors: rationale for dual and multi-antagonists. *J. Med. Chem.* **2014**, *57*, 6301-6315.

[12] Kapp, T.G.; Rechenmacher, F.; Neubauer, S.; Maltsev, O.V.; Cavalcanti-Adam, E.A.; Zarka, R.; Reuning, U., Notni, J.; Jürgen Wester, H.; Mas-Moruno, C.; Spatz, J.; Geiger, B.; Kessler, H. Comprehensive evaluation of the activity and selectivity profile of ligands for RGD-binding integrins *Scientific Reports*, **2017**, *7*, 39805; doi: 10.1038/srep39805.

[13] Miller, L.M.; Pritchard, J.M.; Macdonald, S.J.F.; Jamieson, C.; Watson, A.J.B. Emergence of small molecule non-RGD-mimetic inhibitors for RGD integrins *J. Med. Chem.* **2017**, *60*, 3241-3251.

[14] Cirkek, G. A.; Kerklaan, B. M.; Vanhoutte, F.; Der Aa, A. V.; Lorenzon, F.; Namour, F.; Pujuguet, P.; Darquenne, S.; De Vos, F. Y. F.; Snijders, T. J.; Voest, E. E.; Schellens, J. H. M.; Lolkema, M. P. A dose escalating phase I study of GLPG0187 a broadspectrum integrin receptor antagonist, in adult

patients with progressive high-grade glioma and other advanced solid malignancies. *Investigational New Drugs*, **2016**, *34*, 184-192.

[15] Procopiou, P.A.; Anderson, N.A.; Barrett, J.; Barrett, T.N.; Crawford, M.H.J.; Fallon, B.J.; Hancock, A.P.; Le, J.; Lemma, S.; Marshall, R.P.; Morrell, J.; Pritchard, J.; Rowedder, J.E.; Saklatvala, P.; Slack, R.J.; Sollis, S.L.; Suckling, C.J.; Thorp, L.R.; Vitulli, G.; Macdonald, S.J.F. Discovery of (S)-3-(3-(3,5-dimethyl-1H-pyrazol-1-yl)phenyl)-4-((R)-3-(2-(5,6,7,8-tetrahydro-1,8-naphthyridin-2-yl)ethyl)pyrrolidin-1-yl)butanoic acid, a nonpeptidic αvβ6 integrin inhibitor for the inhaled treatment of idiopathic pulmonary fibrosis. *J. Med. Chem*. **2018**, *61*, 8417-8443.

[16] Weinreb, P. H.; Simon, K. J.; Rayhorn, P.; Yang, W. J.; Leone, D. R.; Dolinski, B. M.; Pearse B. R.; Yokota, Y.; Kawakatsu, H.; Atakilit, A.; Sheppard, D.; Violette, S. M. Function-blocking integrin $\alpha_v\beta_6$ monoclonal antibodies: distinct ligand-mimetic and non-ligand-mimetic classes. *J. Biol. Chem*. **2004**, *279*, 17875-17997.

[17] Maden, C.H.; Fairman, D.; Chalker, M.; Costa, M.J.; Fahy, W.A.; Garman, N.; Lukey, P.T.; Mant, T.; Parry, S.; Simpson, J.K.; Slack, R.J.; Kendrick, S.; Marshall, R.P. Safety, tolerability and pharmacokinetics of GSK3008348, a novel integrin avb6 inhibitor in healthy participants *Eur. J. Clin. Pharm*. **2018**, *74*, 701-709.

[18] Anderson, N. A.; Campbell, I. B.; Fallon B. J.; Lynn, S. M.; Macdonald, S. J. F.; Pritchard, J. M.; Procopiou, P. A.; Sollis, S. L.; Thorp, L. R. Synthesis and determination of absolute configuration of a non-peptidic $\alpha_v\beta_6$ integrin antagonist for the treatment of idiopathic pulmonary fibrosis. *Org. Biomol. Chem*. **2016**, *14*, 5992-6009.

[19] A betaine is a neutral molecule with a positively charged quaternary ammonium group and a negatively charged carboxylate group.

[20] The optical rotation for **7** is $[\alpha]_D^{21} = +11^o$ (c=1.0 in EtOH) and for **8** is $[\alpha]_D^{21} = +2^o$ (c=1.0 in EtOH).

[21] Schrödinger Release 2018-3: MacroModel, Schrödinger, LLC, New York, NY, 2018.

[22] Gaussian 16, Revision B.01, Frisch, M.J.; Trucks, G.W.; Schlegel, H.B.; Scuseria, G.E.; Robb, M.A.; Cheeseman, J.R.; Scalmani, G.; Barone, V.; Petersson, G.A.; Nakatsuji, H.; Li, X.; Caricato, M.; Marenich, A.V.; Bloino, J.; Janesko, B.G.; Gomperts, R.; Mennucci, B.; Hratchian, H.P.; Ortiz, J.V.; Izmaylov, A.F.; Sonnenberg, J.L.; Williams-Young, D.; Ding, F.; Lipparini, F.; Egidi, F.; Goings, J.; Peng, B.; Petrone, A.; Henderson, T.; Ranasinghe, D.; Zakrzewski, V.G.; Gao, J.; Rega, N.; Zheng, G.; Liang, W.; Hada, M.; Ehara, M.; Toyota, K.; Fukuda, R.; Hasegawa, J.; Ishida, M.; Nakajima, T.; Honda, Y.; Kitao, O.; Nakai, H.; Vreven, T.; Throssell, K.; Montgomery, Jr., J.A.; Peralta, J.E.; Ogliaro, F.; Bearpark, M.J.; Heyd, J.J.; Brothers, E.N.; Kudin, K.N.; Staroverov, V.N.; Keith, T.A.; Kobayashi, R.; Normand, J.; Raghavachari, K.; Rendell, A.P.; Burant, J.C.; Iyengar, S.S.; Tomasi, J.; Cossi, M.; Millam, J.M.; Klene, M.; Adamo, C.; Cammi, R.; Ochterski, J.W.; Martin, R.L.; Morokuma, K.; Farkas, O.; Foresman, J.B.; Fox, D.J. Gaussian, Inc., Wallingford CT, 2016.

[23](a) Becke, A.D. Density-functional thermochemistry. III. The role of exact exchange, *J. Chem. Phys.* **1993**, 98, 5648-5652; (b) Lee, C.; Yang W.; Parr, R.G. Development of the Colle-Salvetti correlation-energy formula into a functional of the electron density, *Phys. Rev. B* **1988**, *37*, 785-789; (c) Vosko, S.H.; Wilk, L.; Nusair, M. Accurate spin-dependent electron liquid correlation energies for local spin density calculations: a critical analysis, *Can. J. Phys*. **1980**, 58, 1200-1211; (d) Grimme, S.; Antony, J.; Ehrlich, S.; Krieg, H. A consistent and accurate *ab initio* parametrization of density functional dispersion correction (DFT-D) for the 94 elements H-Pu, *J. Chem. Phys.* **2010**, *132*, 154104.

[24] Tomasi, J.; Mennucci, B.; Cammi, R. Quantum mechanical continuum solvation models, *Chem. Rev*. **2005**, *105*, 2999-3093.

[25] (a) Hariharan, P.C.; Pople, J.A. Influence of polarization functions on molecular-orbital hydrogenation energies, *Theor. Chem. Acc.* **1973**, 28, 213-222; (b) Francl, M.M.; Pietro, W. J.; Hehre, W.J.; Binkley, J.S.; DeFrees, D.J.; Pople, J.A.; Gordon, M.S. Self-consistent molecular orbital methods. 23. A polarization-type basis set for 2nd-row elements, *J. Chem. Phys.* **1982**, 77, 3654-3665; (c) Clark, T.; Chandrasekhar, J.; Spitznagel, G.W.; Schleyer, P.v.R. Efficient diffuse function-augmented basis-sets for anion calculations. 3. The 3-21+G basis set for 1st-row elements, Li-F, *J. Comp. Chem.* **1983**, *4*, 294-301.

[26] Zouvelekis, D.; Yannakopoulou, K.; Mavridis, I.M.; Antoniadou-Vyza, E. The self-association of the drug acemetacin and its interactions and stabilization with β-cyclodextrin in aqueous solution as inferred from NMR spectroscopy and HPLC studies, *Carbohydrate Res*., **2002**, 337, 1387-1395

[27] Rowedder, J. E.; Ludbrook, S. B.; Slack, R. J. Determining the true selectivity profile of α_v integrin ligands using radioligand binding: applying an old solution to a new problem. *SALAS Discovery*, **2017**, *22*, 962-973.

[28] Dong, X.; Hudson, N.E.; Lu, C.; Springer, T.A. Structural determinants of integrin β-subunit specificity for latent TGF-β *Nature Struct. Mol. Biol*. **2014**, *21*, 1091-1097.

[29] Xiong, JP.; Stehle, T.; Zhang, R.; Joachimiak, A.; Frech, M.; Goodman, SL.; Arnaout MA. Crystal structure of the extracellular segment of integrin alpha Vbeta3 in complex with an Arg-Gly-Asp ligand. *Science* **2002**, *5*, 151-155.

[30] Friesner, R.A.; Murphy, R.B.; Repasky, M.P.; Frye, L.L.; Greenwood, J.R.; Halgren, T.A.; Sanschagrin, P.C.; Mainz, D.T., Extra precision Glide: docking and scoring incorporating a model of hydrophobic enclosure for protein-ligand complexes, *J. Med. Chem.*, **2006**, *49*, 6177–6196.

[31] Halgren, T. A.; Murphy, R. B.; Friesner, R. A.; Beard, H. S.; Frye, L. L.; Pollard, W. T.; Banks, J. L., Glide: a new approach for rapid, accurate docking and scoring. 2. Enrichment factors in database screening, *J. Med. Chem.*, **2004**, *47*, 1750–1759.

[32] Friesner, R.A.; Banks, J. L.; Murphy, R. B.; Halgren, T. A.; Klicic, J. J.; Mainz, D. T.; Repasky, M. P.; Knoll, E. H.; Shaw, D. E.; Shelley, M.; Perry, J. K.; Francis, P.; Shenkin, P. S., Glide: a new approach for rapid, accurate docking and scoring. 1. Method and assessment of docking accuracy, *J. Med. Chem.*, **2004**, *47*, 1739–1749.

[33] Gillie, D. J.; Novick, S. J.; Donovan, B. T.; Payne, L. A.; Townsend, C. Development of a high-throughput electrophysiological assay for the human ether-à-go-go related potassium channel hERG. *J. Pharmacol. and Toxicol. Methods*, **2013**, *67*, 33-44.

[34] Harder, E.; Damm, W.; Maple, J.; Wu, C.; Reboul, M.; Xiang, J.Y.; Wang, L.; Lupyan, D.; Dahlgren, M.K.; Knight, J.L.; Kaus, J.W.; Cerutti, D.S.; Krilov, G.; Jorgensen, W.L.; Abel R.; Friesner, R.A.

OPLS3: A force field providing broad coverage of drug-like small molecules and proteins, *J. Chem. Theory Comput.* **2016**, *12*, 281–296.

[35] Qui, D.; Shenkin, P.S.; Hollinger, F.P.; Clark Still, W. The GB/SA continuum model for solvation. A fast analytical method for the calculation of approximate Born radii, *J. Phys. Chem. A*, **1997**, *101*, 3005-3014.